UNIVERSIDADE FEDERAL DO RIO GRANDE DO SUL
PROGRAMA DE PÓS-GRADUAÇÃO EM FÍSICA
Tese de Doutorado

Simulações de Sistemas Carregados Confinados[1]

(Simulations of confined charged systems)

Matheus Girotto

Trabalho sob a orientação dos professor Yan Levin e Alexandre Pereira dos Santos.

Porto Alegre
Abril, 2018

[1]Esse trabalho foi parcialmente financiado pelo Conselho Nacional de Desenvolvimento Científico e Tecnológico (CNPq).

Resumo

Nesta tese nós estudamos sistemas quase bidimensionais carregados e confinados por paredes infinitas eletrificadas. Primeiramente nós derivamos o método de Somas de Ewald em 3d e então tomamos o limite para sistemas confinados sem neutralidade de carga. É mostrado que quando os campos das placas são considerados como potenciais externos há um ganho computacional considerável. Para confinamentos metálicos nós resolvemos a Equação de Poisson usando funções de Green periódicas, que nos permite evitar métodos de minimização que calculam as cargas induzidas nos contornos. Aplicando este formalismo para um modelo de rede de liquidos iônicos, nós capturamos a transição de forma da curva de capacitância característica destes sistemas. Finalmente, nós consideramos superfícies polarizáveis com qualquer constante dielétrica, novamente utilizando funções de Green. Neste algoritmo nós separamos a energia de interação iônica da energia de polarização, o que nos permite adaptar nosso método a qualquer técnica de Somas de Ewald 2d presente na literatura científica. Para completude, nós executamos os cálculos para duas placas com discontinuidades dielétricas diferentes.

Abstract

In this Thesis, we study *quasi* bi-dimensional charged systems confined by infinite electrified walls. First we derive the usual 3d Ewald Summation technique and then take the limit for confined non-neutral systems. It is shown that when the plate fields are considered as external potentials, considerable computational gain is achieved. For metallic confined systems we solve Poisson Equation using periodic Green functions, which allows us to avoid minimization procedures to compute the induced charges at the boundaries. Applying this formalism to a lattice model of ionic liquids we capture the capacitance shape transition characteristic of such systems. Finally, we consider polarizable surfaces of any dielectric constant, again using periodic Green functions. In this algorithm we can separate the energy of ionic interactions from polarization energy, which allows the adaptation of our method to any other 2d Ewald Summation technique already on scientific literature. For completeness, we perform calculations for walls with different dielectric discontinuities.

Acknowledgments

Special thanks to my parents, they were important part of this. They, after all, never let me down.

Thanks to Professor Levin, for making me think hard about matters (without him I would never become anything) and to Professor dos Santos, for teaching me how to code and showing me the importance of extreme hard word – that, unfortunately, I am still learning.

Nicolas Pantaleoni made this all possible by taking me to parties, listening to my thoughts and teaching me about real life outside of academia – and he gave me love when I really needed. Patrice Camati was essential for my thesis and for my life. Éder Milton taught me to be a tougher man in a very polite manner. Bruno Verlindo was a very good friend, which I love deeply. Fábio, Felipe and Frederico Brilhante were some kind of role models for me – since they are honest, kind hearted and for some reason very nice to people around them [and they never, never give up(probably this is why I look up to them)]. Márcia Ilha is as important as Prof. Levin, since without her I also would never become anything.

Since there is a little page left, I would like to mention my two scientific heroes: Nikolai Tesla and Albert Einstein. I personally think that they showed what talent allied with absolute dedication can achieve: they changed the world in many ways. Furthermore, we have yet to understanding the reaches of their works, since black holes still a mystery (a consequence of Einstein's theories) and wireless electronics is not absolutely implemented (the dream of the electricity wizard).

Finally, philosophical considerations were pivotal, since physics cannot access all life, and I was supported mainly by Alan F. Chalmers, Friedrich W. Nietzsche and Raymond Smullyan. Thanks very much to them.

Epigraph

- “Towards thee I roll, thou all-destroying but unconquering whale; to the last I grapple with thee; from hell’s heart I stab at thee; for hate’s sake I spit my last breath at thee.” – Captain Ahab in Moby Dick or The White Whale by Herman Mellvile

- “Lá dentro, entendi em parte o que acontecia: os estudantes protestavam contra a polícia e a polícia protestava contra os estudantes – um jogo de cão e gato que não me interessava e do qual não pretendia fazer parte nem como espectador.” – Protagista sem nome em Pilatos de Carlos Heitor Cony

- “The first principle is that you must not fool yourself and you are the easiest person to fool.” — Richard P. Feynman

- “No, no - I think about thinking.” — Douglas R. Hofstadter

- “Aí me curvei ante a força dos fatos, lavei minhas mãos como Pôncio Pilatos.” — Paulo Vanzolino em Samba Erudito

Published Papers

- (1) **Girotto, M.**; dos Santos, A. P.; Levin, Y; Vortex Distribution in a Confining Potential. *Phys. Rev. E* **2013**, *88*, 032118
- (2) **Girotto, M.**; dos Santos, A. P.; Pakter, R.; Levin, Y; Reply to "Comment on 'Vortex distribution in a confining potential"'. *Phys. Rev. E* **2014**, *90*, 026102
- (3) Mattos, A. E. P.; Sombrio, G.; **Girotto, M.**; Franzen, P. L.; Reis, R.; Pereira, M. B.; Boudinov, H ; Photoluminescence Emission from Si Nanocrystals in SiO2 Matrix Obtained by Reactive Sputtering. *ASEM* **2014**, *6*, 1
- (4) **Girotto, M.**; dos Santos, A. P.; Colla, T.; Levin, Y; Yukawa Particles in a Confining Potential. *J. Chem. Phys.* **2014**, *141*, 014106
- (5) **Girotto, M.**; dos Santos, A. P.; Levin, Y; Interaction of Charged Colloidal Particles at the Air-Water Interface. *J. Phys. Chem. B* **2015**, *120*, 5817-5822 **(Special Issue in honour of Prof. William M. Gelbart)**
- (6) dos Santos, A. P.; **Girotto, M.**; Levin, Y; Simulations of Coulomb Systems with Slab Geometry Using an Efficient 3D Ewald Summation Method. *J. Chem. Phys.* **2016**, *144*, 014103 **(Editor's Choice of the Year in 2016)**
- (7) dos Santos, A. P.; **Girotto, M.**; Levin, Y; Simulations of Polyelectrolyte Adsorption to a Dielectric Like-Charged Surface. *J. Phys. Chem. B* **2016**, *120*, 10387-10393
- (8) Colla, T; **Girotto, M.**; dos Santos, A. P.; Levin, Y; Charge Neutrality Breakdown in Confined Aqueous Electrolytes: Theory and Simulation. *J. Chem. Phys.* **2016**, *145*, 094704
- (9) **Girotto, M.**; Colla, T; dos Santos, A. P.; Levin, Y; Lattice Model of an Ionic Liquid at an Electrified Interface *J. Phys. Chem. B* **2017**, *121*, 6408-6415
- (10) **Girotto, M.**; dos Santos, A. P.; Levin, Y; Simulations of Ionic Liquids Confined by Metal Electrodes Using Periodic Green Functions. *J. Chem. Phys.* **2017**, *147*, 074109
- (11) dos Santos, A. P.; **Girotto, M.**; Levin, Y; Simulations of Coulomb Systems Confined by Polarizable Surfaces Using Periodic Green functions *J. Chem. Phys.* **2017**, *147*, 184105
- (12) **Girotto, M.**; Malóssi, R. M.; dos Santos; A. P., Levin, Y; Lattice model of ionic liquid confined by metal electrodes *J. Chem. Phys.* **2018**, *148*, 193829

Contents

1 Introduction

The first simulations of physical systems date back to the beginning of the twentieth century [1, 2], before the invention of electronic computers. The main rudimentary idea was to arrange macroscopic balls in a chamber and make them interact in a mechanical way that resembled the atomic system of interest [3]. Unfortunately, these methods have intrinsic limitations streaming from the fact that the analysis of the data was very time demanding and complex. Nevertheless, some of these techniques yielded very realistic results.

Then electronic vaulted computers became unclassified, after Second World War, and one machine with research purposes was assembled at Los Alamos by Von Neumann *et al* [4]. Previously, however, there were classified projects, which used fast computing machines for war purposes - for example, calculating thermodynamical properties of nuclear bombs. The new powerful machinery was called MANIAC and attracted the interest of Metropolis, the Rosenbluth couple and the Teller couple. In order to test and use the new tool, Metropolis *et al.* invented a revolutionary algorithm, nowadays known as Metropolis Algorithm, to simulate a bi-dimensional system of hard spheres, and compare it with theoretical predictions using virial expansions [5](The agreement was obtained to a fairly good precision already at those times). This was the beginning of a revolution in all fields of physics, but specially in chemical physics, that is still happening.

Following Metropolis *et al.*, it is known today that Fermi, Pasta and Ulam performed numerical analysis using methods similar to what is now modern molecular dynamics, investigating non-linear systems [6]. The team concluded that a model of 64 atoms with varying harmonic couplings between them does not obey equipartition of energy at equilibrium. Their conclusion, unfortunately, was limited by the power of the machine used. Soon after, the previous reluctance about the machinery that performed incredibly fast arithmetic was abandoned, and the first realistic problems were attacked. One cornerstone of computer science applied to physics was the watershed work of Rahman [7], which shed light in the properties of liquid argon. The world was fated to not be the same anymore, and practically any branch of physics relies on sophisticated computer techniques now.

The revolution on miniaturizing silicon-based transistors opened the doors for a broader use of computer machines in academic media, and computers took a fundamental role in all science - medicine, biology, chemistry etc. Nevertheless, all techniques rely pretty much on the ideas of the pioneers of the field.

Particularly, the use of computers to simulate electric charged system is still an ongoing challenge in technology. Nonetheless, since must of the building blocks of Nature has a Coulombic charge, the efficient simulation of these systems are of paramount importance for modern industry

and science. The difficulty, however, is due to the long-range nature of the electrostatic force, which prevents the use of simple periodic boundary conditions in the main simulation box. For potentials that are short-ranged, as the Yukawa potential, the main cell is replicated only a few times, since the contributions of other replicas become negligible. However, Coulomb forces extend to infinity. In mathematical terms, this means that the electrostatic potential has not a integrable tail and there is no threshold distance beyond which the force is considered to vanishes. Therefore, we must consider one main simulation box interacting with infinite replicas of itself, in order to access the thermodynamical limit. In practice, we have to evaluate a infinite series that is conditionally convergent – depends on the way the replicas are summed –, as long as the overall system is neutral. For systems with a bare electric charge intrinsic divergences arises, that must be renormalized away [8]. The success of computing these series for neutral systems was first achieved by Ewald Summation methods [9], when calculating the bulk energy of ionic crystals to obtain the Madelung constant. Then the technique was improved by a myriad of extensions [3, 10–16]. The main idea behind the algorithm is to separate the potential of a point charge into long and short-ranged contributions, and then compute the former in the reciprocal lattice and the last in the real space.

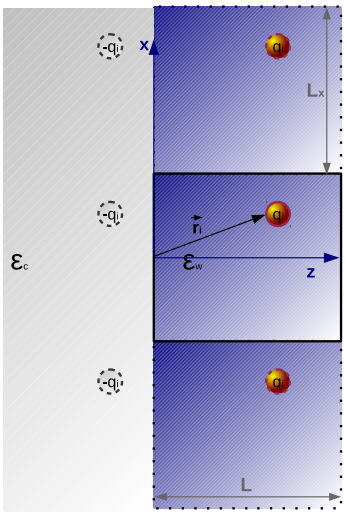

Figure 1: Representation of a system with only one boundary. The Dirichlet and Neumann conditions are easily satisfied by a simple single image construction.

Unfortunately, when there is a broken symmetry, such as finitude of the system in one direction, Ewald Summation loses much of its power. The extra challenge comes from the fact that in Ewald techniques part of the energy is computed in the Fourier space, and a two dimensional transformation of the long range potential leads to the appearance of special functions and to slow convergence of the series [17, 18]. This notwithstanding, many system of interest present a *quasi* bi-dimensional geometry: ionic liquids at electrified interfaces [19–24], charged

nanopores [25–27], nanoconfined electrolytes [28–30], to cite just a handful of examples. Besides, these systems present new interesting phenomena, as like-charged attraction [29,31–35] and charge reversal [36–38], which may be very hard to capture theoretically [39]. In order to numerically attack these systems, techniques to overcome the difficulties have been developed [16,40–44]. The common idea is to still perform a 3d Ewald Summation, retaining its rapid convergence, but to sum infinitely faster in the infinite dimensions in comparison with the finite one. However, a vacuum between the replicas in the non-periodic direction must be artificially inserted on, then the interaction with the replicas in this dimension becomes sufficiently small. Finally, to account correctly for the conditionally convergent summation, one most add a energetic term that depends on the geometry of the main cell. Following this procedure, successful simulations have been performed and the most usual technique is that of Yeh and Berkowitz(YB) [40]. Nonetheless, the calculations presented in the seminal paper by YB are not clear and lack theoretical rigor in the opinion of the author, though its practical efficiency is unquestionable. Pursuing a more efficient simulation for charged systems confined by electrified planar boundaries, Levin *et al.* [8,45] were able to straightforward and clearly derive a 3d Ewald Summation algorithm for bulk *and* slab geometry. In addition, for reduced 2d+h geometries, Levin and coworkers gained substantial computational time (up to one order of magnitude) considering the fields of the plates as external potentials acting on the confined ions. In this thesis, we present a fully detailed explanation of the algorithm with tricks of the trade for its implementation.

As above, the challenges may go a step further, if the charged liquid is confined by polarizable planar surfaces, such as phospholipid membranes or charged carbon planar sheets. It is worth noting, however, that if there is only one wall, see Fig. 1, it is straightforward to extend Ewald Summation methods [46–52]. The simple idea is to consider the image charge of every ion to satisfy the boundary conditions of dielectric discontinuity. Unfortunately, when the system is confined by a pair of surfaces there is no easy extension of the known techniques. The difficulty is due to the fact that the image charge technique requires an infinite number of fictional charges, resulting in a infinite series for every ion of the system. Moreover, since the series is alternating, the way the summation is performed is once again important. Noting that the thermodynamical limit must be accessed, there will be infinite replicas of the ions, resulting in a cumbersome infinite series over the replicas, each one containing an infinite series over the image charges. Despite of the complexity of the problem, both for metal or dielectric confinements, methods to solve it were proposed [20, 53–55]. Considering metal electrodes, the most common algorithms rely on the calculation of induced charges using minimization procedures [20,56,57]. This method is very expensive computationally, since every step of simulation the minimum of a complex energy function must be found – more often using gradient methods. Besides, this sets restrictions on the size of the simulated systems, preventing accurate enough investigations in strongly interacting

fluids. Also, there are methods that use the condition of displacement vector discontinuity or sum using brute force the series implied by image charge techniques [58–64]. dos Santos and Levin [28] performed an efficient image charge summation for dielectric boundaries, though the convergence rate deteriorates with the dielectric contrast γ. The efficiency of these methods are very poor for dense and extremely interacting fluids, such as room temperature ionic liquids – thus the simulations of such systems still an ongoing defiance for physicists and chemists alike. Nonetheless, ionic liquids are promising materials [19, 65], with applications in distinct technologies, such as supercapacitors [66–69], solar cells [70, 71] and others renewable energy devices [72, 73]. Thus, a broad understanding of these liquids is essential for science and engineering.

Quite recently, however, Levin *et al.* [74, 75] developed and applied totally new approaches that use periodic Green functions as solutions to the Poisson Equation. The main advantage is that the calculation of the induced charge on the polarizable walls are trivial and performed on the fly, requiring the solution of a linear equation only. In this thesis we present both methods, pointing its advantages and drawbacks, as well as its applications to electrolytes and ionic liquids. We show that these algorithms are very efficient and can be further used for tackling previous computationally prohibitive systems.

This thesis is organized as follows: first we derive 3d Ewald Summation and then take the limit for slab geometry and non-neutral systems with applied external electric fields. We see that for the two-dimensional geometry with confining electrified plates, the approach may be 10 times faster than usual algorithms. Furthermore, this method yields exactly the same results of other procedures. Second, we develop a new method for charged systems bounded by metallic planar surfaces. In this framework we can calculate very rapidly the induced charges, also the resulting potential of a point charge decays exponentially, allowing us to perform a fast convergent summation in real space only. In addition, we applied this formalism to a lattice model of room temperature ionic liquids, showing that our very simple model captures the shape transition between camel to bell-shaped capacitance curve [19]. The simulations can be made more rapid by precalculating the potentials in the lattice sites before the beginning of the Metropolis Algorithm. Third, we consider a more general system, where any pair of planar confinements is solved. Besides, we show that we can decouple the energy of polarization from the ionic interactions, making our algorithm easily combined with any other in the market. Fourth, one last, definitive step is taken, where two confining surfaces are considered with different dielectric constants, ϵ_1 and ϵ_2; the author is not aware of any other method in the chemical computer science that accounts for this complicated configuration. Finally, conclusions are presented and future work discussed.

2 Ewald Summation for bulk and slab geometry

We first derive energy formulæ for a non-neutral charged system at the bulk. We consider a system of N particles with charges q^j located at random positions $\boldsymbol{r}^j$ in a simulation box with lengths L_x, L_y and L_z, see Fig. 2. In order to replicate the cell in all directions we define the replication vector as $\boldsymbol{r}_{ep} = (m_x L_x, m_y L_y, m_z L_z)$, where m's spam the integers, $(m_x, m_y, m_z) \in \mathbb{Z}$. The electrostatic potential generated by the ions and all of its replicas at point P, also located at random position $\boldsymbol{r}$, can be generally written as

$$\phi(\boldsymbol{r}) = \sum_{\boldsymbol{m}}^{\infty} \sum_{j=1}^{N} \int \frac{\rho^j(\boldsymbol{s})}{\epsilon_w |\boldsymbol{r} - \boldsymbol{s}|} d^3\boldsymbol{s} \ , \tag{2.1}$$

where $\rho^j(\boldsymbol{s}) = \mathrm{q}^j \delta(\boldsymbol{s} - \boldsymbol{r}^j - \boldsymbol{r}_{ep})$ is the charge density of q^j and its replicas. The summation over $\boldsymbol{m}$ includes the central simulation box, corresponding to $\boldsymbol{m} = (0,0,0)$. To efficiently handle this conditionally convergent series we use Ewald 3d Summation method. The main idea of the algorithm is to split the Coulombic potential into short and long-ranged potentials, thus computing the later in the Fourier space. To perform the separation we add and subtract a Gaussian charge distribution centered at each particle, then we can write

$$\phi(\boldsymbol{r}) = \sum_{\boldsymbol{m}}^{\infty} \sum_{j=1}^{N} \int \frac{\rho^j(\boldsymbol{s}) - \rho^j_G(\boldsymbol{s})}{\epsilon_w |\boldsymbol{r} - \boldsymbol{s}|} d^3\boldsymbol{s} + \sum_{\boldsymbol{m}}^{\infty} \sum_{j=1}^{N} \int \frac{\rho^j_G(\boldsymbol{s})}{\epsilon_w |\boldsymbol{r} - \boldsymbol{s}|} d^3\boldsymbol{s} \ , \tag{2.2}$$

where $\rho^j_G(\boldsymbol{s}) = \mathrm{q}^j (\kappa_e^3/\sqrt{\pi^3}) \exp\left(-\kappa_e^2 |\boldsymbol{s} - \boldsymbol{r}^j - \boldsymbol{r}_{ep}|^2\right)$ and κ_e is a damping parameter. Note that $\rho^j_G(\boldsymbol{s})$ integrates to q^j. We can rewrite the potential using the Error Functions, resulting in

$$\phi(\boldsymbol{r}) = \sum_{\boldsymbol{m}}^{\infty} \sum_{j=1}^{N} \mathrm{q}^j \frac{\mathrm{erf}(\kappa_e |\boldsymbol{r} - \boldsymbol{r}^j - \boldsymbol{r}_{ep}|)}{\epsilon_w |\boldsymbol{r} - \boldsymbol{r}^j - \boldsymbol{r}_{ep}|} + \sum_{\boldsymbol{m}}^{\infty} \sum_{j=1}^{N} \mathrm{q}^j \frac{\mathrm{erfc}(\kappa_e |\boldsymbol{r} - \boldsymbol{r}^j - \boldsymbol{r}_{ep}|)}{\epsilon_w |\boldsymbol{r} - \boldsymbol{r}^j - \boldsymbol{r}_{ep}|} \ , \tag{2.3}$$

where $\mathrm{erf}(x)$ is the Error Function and $\mathrm{erfc}(x)$ is the Complementary Error Function. The second term on Eq. 2.3 is short-ranged and can be computed in the usual way for potentials with an integrable tail. We can Fourier transform the first term and write

$$\phi(\boldsymbol{r}) = \sum_{\boldsymbol{k}=\boldsymbol{0}}^{\infty} \sum_{j=1}^{N} \frac{4\pi \mathrm{q}^j}{\epsilon_w V |\boldsymbol{k}|^2} \exp\left[-\frac{|\boldsymbol{k}|^2}{4\kappa_e^2} + i\boldsymbol{k} \cdot (\boldsymbol{r} - \boldsymbol{r}^j)\right] + \sum_{j=1}^{N} \mathrm{q}^j \frac{\mathrm{erfc}(\kappa_e |\boldsymbol{r} - \boldsymbol{r}^j|)}{\epsilon_w |\boldsymbol{r} - \boldsymbol{r}^j|} \ , \tag{2.4}$$

where $\boldsymbol{k} = (\frac{2\pi}{L_x} m_x, \frac{2\pi}{L_y} m_y, \frac{2\pi}{L_z} m_z)$. In the second term of Eq. 2.4 we removed the summation over replicas, considering only the main box, $\boldsymbol{m} = (0,0,0)$, with the usual periodic boundary condition. This is justified when κ_e is sufficiently large, so that $\mathrm{erfc}(\kappa_e |\boldsymbol{r} - \boldsymbol{r}^j|)$ decays rapidly, and the minimum image convention can be used where just the first neighbor cells are considered [10]. Unfortunately, for $\boldsymbol{k} = (0,0,0)$, the first term on the right of Eq. 2.4 diverges. Large discussions have been devoted to it in literature [3,10,16,44,76,77]. The more commonly accepted argument is that the so-called *tinfoil boundary* must be considered, where induced charges would compensate

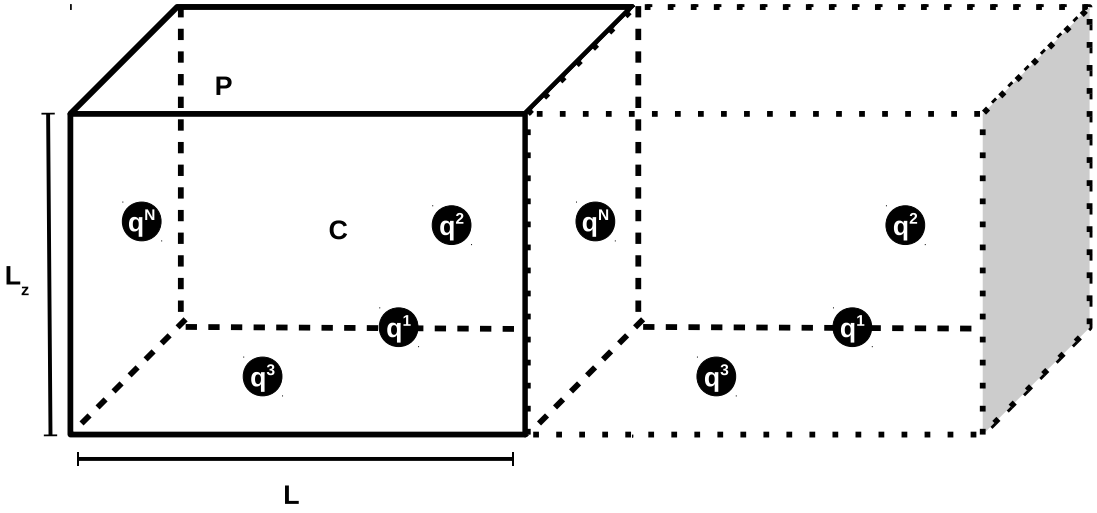

Figure 2: The simulation box with randomly positioned charges and one of its replicas. The point C represents the center of the simulation box, where the origin is located, and P a random point. In charged systems the cell is replicated infinitely.

for the infinities. However, a system that is infinite cannot have any boundary at all, since it occupies all space. Furthermore, the introduction of an artificial boundary is inconsistent with the infinitely periodic system implicit in Ewald Summation technique. Clearly the series evaluation can be performed in the real space, and though is conditionally convergent, it has a *well defined* value for a method of summation – spherical, planewise and others. Real and reciprocal space summations have to agree, otherwise a blatant inconsistency arises – and this is the case if the $\boldsymbol{k} = (0,0,0)$ is simply ignored. Nonetheless, its is taken for grant that charge neutrality and tinfoil boundary conditions make the term vanishes, though there is no *a priori* reason for it. Fortunately, this recklessness seems to not introduce large errors in bulk systems, so the measured observables does not change. However, for systems with reduced geometry, such as slab geometry, the neglecting of the $\boldsymbol{k} = \mathbf{0}$ contribution can lead to significant errors [40]. Considering the term in more detail, we write

$$\lim_{\boldsymbol{k}\to 0} \sum_{j=1}^{N} \frac{4\pi q^j}{\epsilon_w V |\boldsymbol{k}|^2} \exp\left[-\frac{|\boldsymbol{k}|^2}{4\kappa_e^2}\right] \exp\left[+i\boldsymbol{k}\cdot(\boldsymbol{r}-\boldsymbol{r}^j)\right] , \tag{2.5}$$

then we expand the exponentials and ignore the *constant* prefactors, leaving us with

$$\lim_{\boldsymbol{k}\to 0} \sum_{j=1}^{N} \mathrm{q}^j \frac{1}{|\boldsymbol{k}|^2} - \sum_{j=1}^{N} \mathrm{q}^j \frac{1}{4\kappa_e^2} + \lim_{\boldsymbol{k}\to 0} \sum_{j=1}^{N} \mathrm{q}^j \frac{i\boldsymbol{k}\cdot(\boldsymbol{r}-\boldsymbol{r}^j)}{|\boldsymbol{k}|^2} - \lim_{\boldsymbol{k}\to 0} \sum_{j=1}^{N} \mathrm{q}^j \frac{[\boldsymbol{k}\cdot(\boldsymbol{r}-\boldsymbol{r}^j)]^2}{2|\boldsymbol{k}|^2} + \mathcal{O}(|\boldsymbol{k}|) , \tag{2.6}$$

and we point that the higher order terms are "dragged" to zero by the powers of $|\boldsymbol{k}|$. The first two terms can be renormalized away with a redefinition of the zero potential, since they tend towards infinity and are position *independent*. Also, if the system is charge neutral, $\sum_j \mathrm{q}^j = 0$,

both terms vanish. The renormalization process is akin to the one performed to calculate the electrostatic potential of a infinite planar charged sheet. However, for the third and fourth terms of Eq. 2.6 great caution is needed, and the correct limits must be taken properly. We use Dirac delta functions to rewrite the terms and then control the divergences by the limits of integration introduced. Then, considering the third term, we write

$$S_3 = \sum_{j=1}^{N} \mathrm{q}^j \int_{-\infty}^{+\infty} \delta(\boldsymbol{k}) \frac{i\boldsymbol{k}\cdot(\boldsymbol{r}-\boldsymbol{r}^j)}{|\boldsymbol{k}|^2} d\boldsymbol{k} \ , \tag{2.7}$$

with the following representation of the delta function

$$\delta(\boldsymbol{k}) = \frac{1}{(2\pi)^3} \int_{-\boldsymbol{H}}^{\boldsymbol{H}} e^{i\boldsymbol{k}\cdot\boldsymbol{p}} d^3p \ . \tag{2.8}$$

The limits of integration, $-\mathbf{H}$ to $\mathbf{H}$, where $\mathbf{H} = (H_1, H_2, H_3)$, must be performed corresponding to the way that the sum is computed in the real space. Note that this representation of delta function encodes the behavior of the macroscopic aspect ratio, because of the dependence of the limits on how the system is constructed. For example, if we replicate the cell in a spherically symmetric fashion, then $H_1 = lim_{m\to\infty} mL_x$, $H_2 = lim_{m\to\infty} mL_y$, and $H_3 = lim_{m\to\infty} mL_z$, that is, all sides diverge at the same rate. These limiting processes construct a macroscopic cubic system if $L_x = L_y = L_z$. In another example, if $L_z = 2L_y = 2L_x$, we wind up with a macroscopic rectangular system. However, for slab geometry H_1 and H_2 should go to infinity infinitely faster than H_3. This way we construct a system that is infinitely larger in x and y directions. In general it is convenient to define $H_1 = \alpha_1 L_c$, $H_2 = \alpha_2 L_c$ and $H_3 = \alpha_3 L_c$, where L_c is some characteristic macroscopic length scale. The integrals over p_1, p_2 and p_3 in Eq. 2.8 can be performed explicitly yielding the following representation of the delta function,

$$\delta(\boldsymbol{k}) = \frac{1}{(2\pi)^3} \prod_{i=1}^{3} \int_{-\alpha_i \frac{L_c}{2}}^{\alpha_i \frac{L_c}{2}} e^{ik_i p_i} dp_i = \frac{1}{\pi^3} \prod_{i=1}^{3} \frac{\sin(k_i \alpha_i L_c/2)}{k_i} \ . \tag{2.9}$$

The above equation expresses the large distance feature of the lattice sum and is at the heart of the singular behavior of the $\boldsymbol{k} \to 0$ limit. Eq. 2.7 can then be written as $S_3 = \sum_{j=1}^{N} q_j \boldsymbol{D}\cdot(\boldsymbol{r}-\boldsymbol{r}^j)$, where the components of the $\boldsymbol{D}$ vector are

$$D_n = \frac{i}{\pi^3} \int_{-\infty}^{+\infty} \frac{k_n}{|\boldsymbol{k}|^2} \prod_{j=1}^{3} \frac{\sin(k_j \alpha_j L_c/2)}{k_j} d^3\boldsymbol{k} \ , \tag{2.10}$$

that vanish by symmetry, $D_n = 0$, thus $S_3 = 0$. The fourth non-vanishing term of Eq. 2.6 is

$$S_4 = -\sum_{j=1}^{N} \mathrm{q}^j \int_{-\infty}^{+\infty} \delta(\boldsymbol{k}) \frac{[\boldsymbol{k}\cdot(\boldsymbol{r}-\boldsymbol{r}^j)]^2}{2|\boldsymbol{k}|^2} d^3\boldsymbol{k} \ , \tag{2.11}$$

where we again use the delta function representation to rewrite the term,

$$S_4 = -\sum_{j=1}^{N} \frac{\mathrm{q}^j}{2\pi^3} \sum_{n=1}^{3} B_n (r_n - r_n^j)^2 \ , \tag{2.12}$$

where r_n's are components of position vector and B_n can be written as

$$B_n = \int_{-\infty}^{+\infty} d^3\boldsymbol{k} \frac{k_n^2}{|\boldsymbol{k}|^2} \prod_{j=1}^{3} \frac{\sin(k_j \alpha_j L_c/2)}{k_j} \ . \tag{2.13}$$

Fortunately this integral can be reformulated in a convenient form, where first we use the identity

$$\frac{1}{|\boldsymbol{k}|^2} = \int_0^{\infty} dt' \ e^{-t'|\boldsymbol{k}|^2} \ , \tag{2.14}$$

and change variables so it is easier to handle the integrals in the limit of slab geometry, though the equations are still quite general. The variable change is

$$\frac{1}{\sqrt{t}} = \frac{L_c \alpha_3}{2\sqrt{t'}} \ , \tag{2.15}$$

thus the coefficients B_n can be simplified to [78]

$$B_1 = \frac{\pi^{\frac{5}{2}}}{2} \int_0^{+\infty} \frac{\alpha_{13} e^{-\frac{\alpha_{13}^2}{4t}} \mathrm{erf}(\frac{\alpha_{23}}{2\sqrt{t}}) \mathrm{erf}(\frac{1}{2\sqrt{t}})}{t^{\frac{3}{2}}} dt \ , \tag{2.16}$$

$$B_2 = \frac{\pi^{\frac{5}{2}}}{2} \int_0^{+\infty} \frac{\alpha_{23} e^{-\frac{\alpha_{23}^2}{4t}} \mathrm{erf}(\frac{\alpha_{13}}{2\sqrt{t}}) \mathrm{erf}(\frac{1}{2\sqrt{t}})}{t^{\frac{3}{2}}} dt \ , \tag{2.17}$$

$$B_3 = \frac{\pi^{\frac{5}{2}}}{2} \int_0^{+\infty} \frac{e^{-\frac{1}{4t}} \mathrm{erf}(\frac{\alpha_{13}}{2\sqrt{t}}) \mathrm{erf}(\frac{\alpha_{23}}{2\sqrt{t}})}{t^{\frac{3}{2}}} dt \ , \tag{2.18}$$

where $\alpha_{ij} = \alpha_i/\alpha_j$ are the aspect ratios of the macroscopic system. The coefficients B_n's can be calculated using numerical integration. For instance, if a spherical summation is performed, we have for the aspect ratios $\alpha_{13} = L_x/L_z$ and $\alpha_{23} = L_y/L_z$, then we are at *bulk* regime. On the other hand, for a slab planewise summation we have divergences, $\alpha_{13} = \alpha_{23} = \infty$. However, in this limit, the integrals of $\boldsymbol{B}$ can be performed explicitly, yielding $B_1 = B_2 = 0$ and $B_3 = \pi^3$. Note that in this way we avoid an explicit 2d Fourier transformation, first performing a general calculation on the three-dimensional space and then taking a limit, choosing proper aspect ratios. Separating the $\mathbf{k} = \mathbf{0}$ term and putting it in evidence, we can write the renormalized potential as

$$\Delta\phi(\boldsymbol{r}) = \sum_{\boldsymbol{k}\neq\mathbf{0}}^{\infty} \sum_{j=1}^{N} \frac{4\pi \mathrm{q}^j}{\epsilon_w V |\boldsymbol{k}|^2} \exp\left[-\frac{|\boldsymbol{k}|^2}{4\kappa_e^2} + i\boldsymbol{k}\cdot(\boldsymbol{r} - \boldsymbol{r}^j)\right] - \sum_{j=1}^{N} \sum_{n=1}^{3} \frac{2\mathrm{q}^j}{\epsilon_w V \pi^2} B_n (r_n - r_n^j)^2 + \sum_{j=1}^{N} \mathrm{q}^j \frac{\mathrm{erfc}(\kappa_e |\boldsymbol{r} - \boldsymbol{r}^j|)}{\epsilon_w |\boldsymbol{r} - \boldsymbol{r}^j|} \ , \tag{2.19}$$

where Δ corresponds to the renormalization of the potential in Eq. 2.4 – subtraction of infinite constant. Note that, even for charge neutral isotropic bulk systems, Eq. 2.19 is different from the usual formula found in the literature [3, 10, 40]. The difference is the appearance of a term that

depends on the way the infinite sum is performed, *i.e*, on the aspect ratios of the macroscopic system. Fortunately, it seems that for such systems the contribution of the term from $\mathbf{k} \to \mathbf{0}$ limit seems to be small when calculating *averages* on the bulk [16, 44]. This may account for the prevalent use of tinfoil boundary conditions which are claimed to eliminate the correction term. Nevertheless, there is no *a priori* reason to ignore the term and a systematical erasing of it may lead to significant errors for systems with different macroscopic aspect ratios. Furthermore, in order to properly describe an electrostatic system in the thermodynamic limit - in particular an inhomogeneous one - using simulations based on the periodic replication of the cell, the singular term is important and cannot in general be neglected.

As a test for the modified Ewald Summation formula, Eq. 2.19, we consider a *non-neutral* system and calculate the potential difference from a random position $\mathbf{r}$ and the center $\mathbf{0}$ of the simulation cell, $\phi(\mathbf{r}) - \phi(\mathbf{0})$. Note that though the electrostatic potential of a periodic non-neutral system is divergent, the potential difference is well defined. We construct a simulation cell with dimensions $L_x = L_y = 1\mathring{A}$ and $L_z = 2\mathring{A}$. A spherical summation will result in a system with aspect ratios $\alpha_{13} = \alpha_{23} = 1/2$, leading to $B_1 = B_2 = 13.5158$ and $B_3 = 3.9746$. The cell has two charges $q_1 = q_2 = |e|$, where $|e|$ is the absolute value of electron charge, located at random positions. Using Eq. 2.19 we find the potential difference, $\Delta\phi = \phi(\mathbf{r}) - \phi(\mathbf{0})$, using 250 $\boldsymbol{k}$-vectors spherically summed, obtaining a precision of two decimal places. In order to find the same accuracy using Eq. 2.1 we needed spherically sum ≈ 19500 $\boldsymbol{m}$-vectors. Therefore, the sum in real space has a much slower convergent rate.

In planar geometry we want to replicate the cell only in two out of three directions, x and y. We can again use Eq. 2.19, but with proper limits for the aspect ratios, $\alpha_{13} = \alpha_{23} = \infty$. Therefore, slab geometry requires that replications in x and y directions should be performed infinitely faster than that in z direction. This condition leads to $B_1 = B_2 = 0$ and $B_3 = \pi^3$. Eq. 2.19 now becomes

$$\Delta\phi(\boldsymbol{r}) = \sum_{\boldsymbol{k}\neq\mathbf{0}}^{\infty}\sum_{j=1}^{N} \frac{4\pi \mathrm{q}^j}{\epsilon_w V|\boldsymbol{k}|^2} \exp\left[-\frac{|\boldsymbol{k}|^2}{4\kappa_e^2} + i\boldsymbol{k}\cdot(\boldsymbol{r}-\boldsymbol{r}^j)\right] - \sum_{j=1}^{N}\frac{2\pi \mathrm{q}^j}{\epsilon_w V}(r_3 - r_3^j)^2 + \sum_{j=1}^{N}\mathrm{q}^j \frac{\mathrm{erfc}(\kappa_e|\boldsymbol{r}-\boldsymbol{r}^j|)}{\epsilon_w|\boldsymbol{r}-\boldsymbol{r}^j|} \ . \tag{2.20}$$

Unfortunately, we still replicate in z direction, then a vacuum in that direction must be artificially inserted, this way preventing that the replicas in this dimension to add to the total electrostatic potential, see Fig. 3. The empty space must be chosen sufficiently large so the extra addition of vacuum does not alter the properties of the system anymore. Intending to test Eq. 2.20 we consider the same two particle system than before. The introduction of the vacuum region is achieved by limiting the initial random positions of the particles and of the vector $\mathbf{r}$ to $-L_z/4 < z < L_z/4$. Using Eq. 2.1 we can explicitly calculate the potential difference $\Delta\phi$ when the simulation cell is replicated only in the x and y directions, using the replica-vectors $\mathbf{m} = (m_x, m_y, 0)$. The convergence is very slow requiring values of 2.5×10^6 replicas to get an accuracy of two decimal

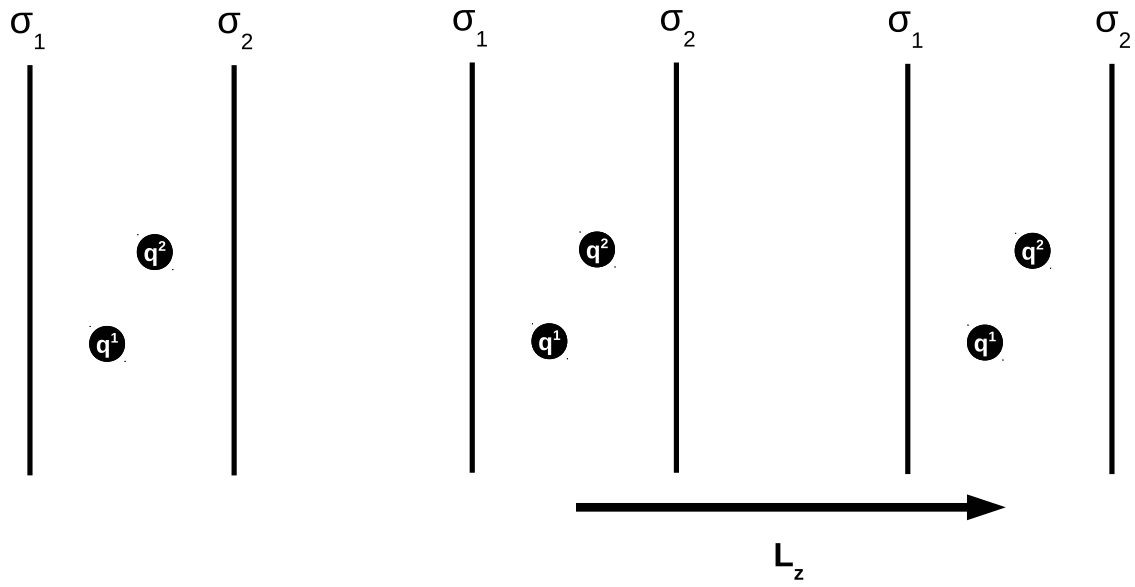

Figure 3: 3d replicated system. Note that inside the central simulation cell the electric fields produced by the z-replication of charged walls cancel out.

places. The same accuracy is achieved with Eq. 2.20 using the vacuum region and only ≈ 650 $\boldsymbol{k}$-vectors.

The renormalized electrostatic energy for a non-neutral slab system can now be calculated with $E = \frac{1}{2}\sum_{i=1}^{N} \mathrm{q}^i \Delta\phi(\boldsymbol{r}^i)$, resulting in

$$E = \sum_{\boldsymbol{k}\neq\boldsymbol{0}}^{\infty} \frac{2\pi}{\epsilon_w V|\boldsymbol{k}|^2} \exp\left[-\frac{|\boldsymbol{k}|^2}{4\kappa_e^2}\right][A(\boldsymbol{k})^2 + B(\boldsymbol{k})^2] + \frac{2\pi}{\epsilon_w V}[M_z^2 - Q_t G_z] + \frac{1}{2}\sum_{i\neq j}^{N} \mathrm{q}^i\mathrm{q}^j \frac{\mathrm{erfc}(\kappa_e|\boldsymbol{r}^i - \boldsymbol{r}^j|)}{\epsilon_w|\boldsymbol{r}^i - \boldsymbol{r}^j|} - \frac{\kappa_e}{\epsilon_w\sqrt{\pi}}\sum_{i}^{N} q_i^2 \ , \qquad (2.21)$$

where

$$\begin{aligned} A(\boldsymbol{k}) &= \sum_{i=1}^{N} \mathrm{q}^i \cos(\boldsymbol{k}\cdot\boldsymbol{r}^i) \ , \\ B(\boldsymbol{k}) &= -\sum_{i=1}^{N} \mathrm{q}^i \sin(\boldsymbol{k}\cdot\boldsymbol{r}^i) \ , \\ M_z &= \sum_{i=1}^{N} \mathrm{q}^i r_3^i \ , \\ Q_t &= \sum_{i=1}^{N} \mathrm{q}^i \ , \\ G_z &= \sum_{i=1}^{N} \mathrm{q}^i (r_3^i)^2 \ . \end{aligned} \qquad (2.22)$$

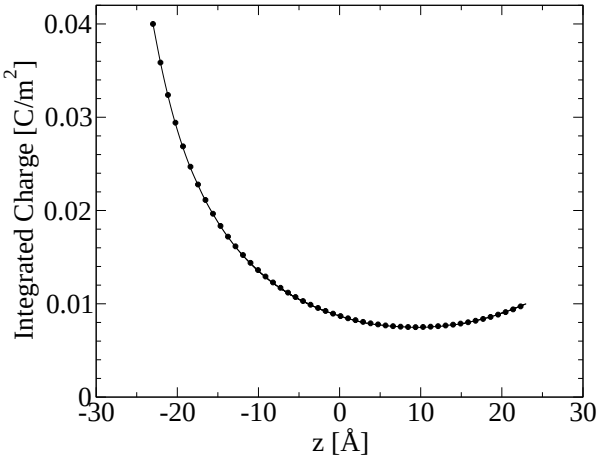

Figure 4: Integrated charge between the plates. Symbols represent the calculation using the modified (non-neutral) 3d Ewald approach, while line, the traditional method [40]. The difference is imperceptible.

The last term on Eq. 2.21 arises when we carefully double sum the long range potential. For a neutral system, $Q_t = 0$, we recover the earlier expression for the electrostatic energy [40]. Now having the total renormalized electrostatic energy we can endow the plates with *constant* superficial charge and treat the produced field as an external potential. This can be successfully achieved because the electric fields of the transverse replicated plates are constant and therefore cancel out, see Fig. 3. Usually, traditional simulations consider the electrified surfaces constructed of point charges, which slows down the simulations, since they must have to be taken into account at every algorithm step. The main idea of our method is to avoid such calculations, considering the plates as external potentials that give rise to an energetic contribution of the form

$$E_p = \frac{2\pi}{\epsilon_w} \sum_{i=1}^{N_c} (\sigma_2 - \sigma_1) r_3^i \mathrm{q}^i \ , \tag{2.23}$$

which must be added to Eq. 2.21. The price one must pay for this is to be able to consider a non-neutral system.

Now we are at position to perform Metropolis algorithm for systems such as nanoconfined ions in slab geometry. Usually such fluids consist of a salt dissolve in water, in a way that the ions dissociate in the medium and each has a total electric charge, such as Na^+ and Cl^-. However, in order to testify the correctness of the method, first we perform simulations in the NVT ensemble using the traditional algorithm (the plates are charged by point particles) and our new method (the plates are external potentials). For the former the surface charge is represented by 256 point particles, thus the overall system is charge neutral, $Q_t = 0$. Here the system has consisted just of counterions, ionic particles that dissociated from the plates and are free to wander between them in the solvent – plus the point charges of the plates for the common algorithm. We set the

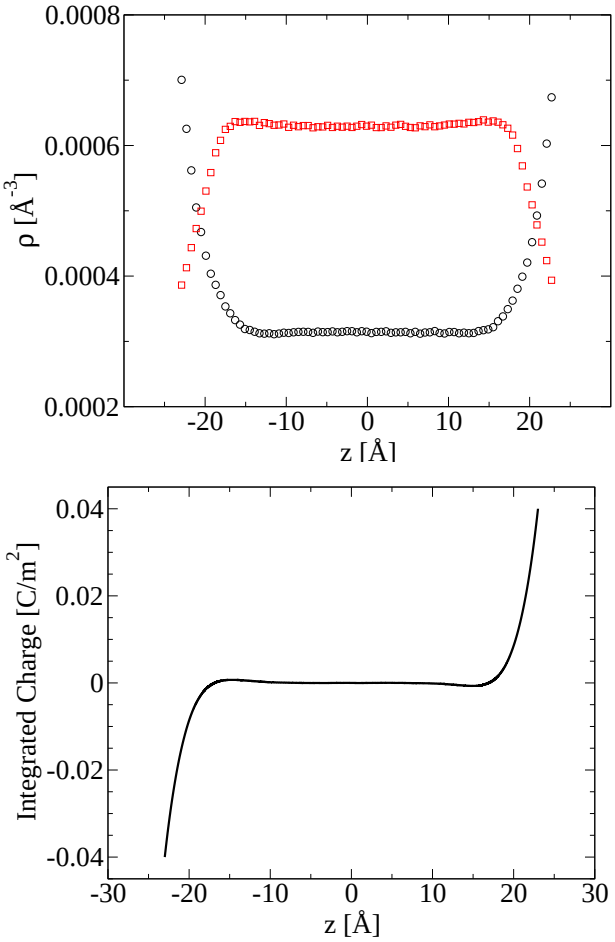

Figure 5: (a) Density profiles of $2:1$ electrolyte confined by charged infinite walls. Circles are anions and squares are cations. (b) The integrated charge.

dimensions of the system at $L_x = L_y = 17,9\text{nm}$ and $L_z = 40\text{nm}$, and the plates are separated by $d = 5\text{nm}$. We consider the counterions as hard spheres with radius $R = 2\text{Å}$. To calculate the Fourier contribution to the energy ≈ 500 $\boldsymbol{k}$-vectors were used and the equilibrium was achieved by 10^6 Monte Carlo steps. The profiles were calculated using 2×10^4 uncorrelated samples after relaxation and the plates have charge $\sigma_1 = 0.04\text{C/m}^2$ and $\sigma_2 = -0.01\text{C/m}^2$, see Fig. 3. In the method of the present chapter we use the superficial charge densities to calculate the number of the counterions, $|\sigma|L_xL_y = N_c|e|$, where N_c is the number of counterions. The results are indistinguishable, see Fig. 4. The computational gain was of one order of magnitude in time in comparison with the corrected 3d Ewald Summation method where the plates are embodied with point charges. Next, we apply the new method for the case $\sigma_1 = \sigma_2 = 0.04\text{C/m}^2$, which is of practical importance when studying colloidal suspension using Derjaguin approximation [79]. In this case we consider electrolyte between the boundaries at concentration of 500mM, both di-valent and quadri-valent, $2:1$ and $4:1$, respectively. Note that there is no external electric field

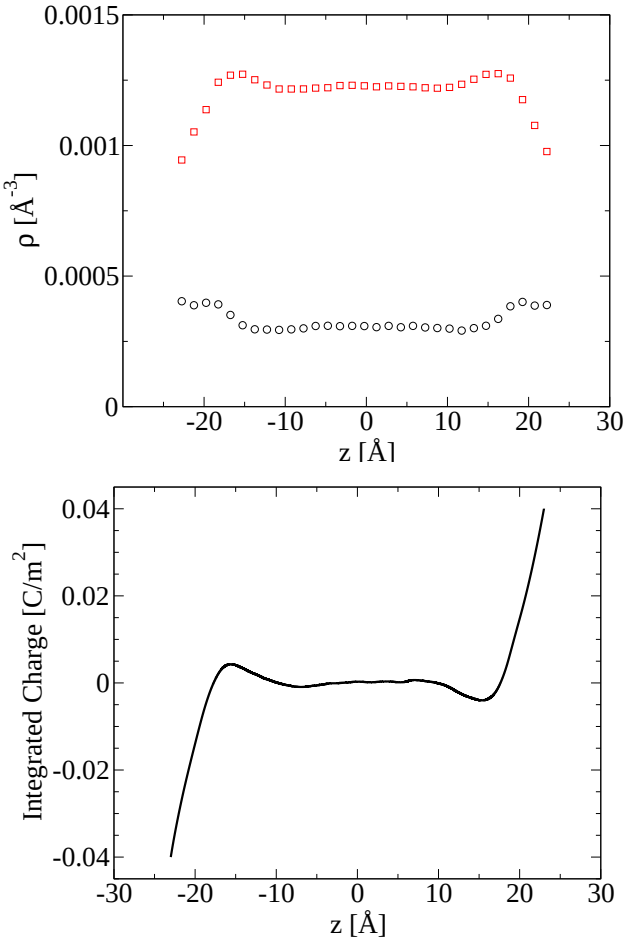

Figure 6: (a) Density profiles of 4 : 1 electrolyte confined by charged infinite walls. Circles are anions and squares are cations. (b) The integrated charge.

in this configuration, since each plate cancels out the other surface field. The values of σ are used only to calculate the number of counterions. The ionic profiles and integrated charge are shown in Fig. 5 and Fig. 6. Observe that for 4 : 1 salt there is a significant charge inversion. This is due to positional correlation between plates and counterions, so the counterions overcompensate the surface charge, see Fig 6. This phenomenon can also occur with divalent counterions, but is considerably weaker, see Fig. 5. A study of such strongly correlated inhomogeneous charged systems is not very practical with other simulation methods.

3 Ionic liquids confined between metal electrodes

We start by calculating the electrostatic potential at position $\boldsymbol{r} = \rho\hat{\boldsymbol{\rho}} + \varphi\hat{\boldsymbol{\varphi}} + z\hat{\boldsymbol{z}}$ produced by a *single* ion of charge q located at $\boldsymbol{r}_0 = z_0\hat{\boldsymbol{z}}$, see Fig. 7, between two parallel grounded infinite metal electrodes. The final solution will be easily generalized to an arbitrary potential difference between the boundaries. We use cylindrical coordinates in order to explore the azimuthal symmetry of the potential, eliminating the φ dependence of it. To obtain the electrostatic potential requires us to solve the Poisson equation [80]

$$\nabla^2\phi(\boldsymbol{r},\boldsymbol{r}_0) = -\frac{4\pi q}{\epsilon}\delta(\boldsymbol{r}-\boldsymbol{r}_0)\ , \tag{3.1}$$

with the Dirichlet boundary condition $\psi_0 = 0$ at each surface. We start by expanding the delta function in the eigenfunctions of the differential operator

$$\frac{d^2\psi_n}{dz^2} + k_n^2\psi_n = 0\ , \tag{3.2}$$

satisfying the boundary conditions $\psi_n(0) = \psi_n(L) = 0$. The eigenfunctions are found to be $\psi_n(z) = \sqrt{2/L}\sin(k_n z)$, with $k_n = n\pi/L$. The Dirac delta function can then be written as

$$\delta(z-z_0) = \frac{2}{L}\sum_{n=1}^{\infty}\sin(\frac{n\pi z}{L})\sin(\frac{n\pi z_0}{L})\,. \tag{3.3}$$

The electrostatic potential can now be build as

$$\phi(\rho,z;z_0) = \frac{2q}{\epsilon L}\sum_{n=1}^{\infty}\sin(\frac{n\pi z}{L})\sin(\frac{n\pi z_0}{L})g_n(\rho)\,. \tag{3.4}$$

Substituting this expression into Eq. 3.1 we obtain an ordinary differential equation for $g_n(\rho)$,

$$\frac{1}{\rho}\frac{\mathrm{d}}{\mathrm{d}\rho}(\rho\frac{\mathrm{d}g_n}{\mathrm{d}\rho}) - k_n^2 g_n = -\frac{2}{\rho}\delta(\rho)\,, \tag{3.5}$$

which has modified Bessel functions of zeroth order as solutions, $g_n(\rho) = AI_0(k_n\rho) + BK_0(k_n\rho)$. Since the potential must vanish as $\rho \to \infty$, the coefficient $A = 0$, while the coefficient B is determined by the singular part of the potential, and is found to be $B = 2$. The electrostatic potential produced by an ion located at $\boldsymbol{r}_0 = z_0\hat{\boldsymbol{z}}$ between two grounded metal surfaces is then [80]

$$\phi(\rho,z;z_0) = \frac{4q}{\epsilon L}\sum_{n=1}^{\infty}\sin(k_n z)\sin(k_n z_0)K_0(k_n\rho)\ . \tag{3.6}$$

We can now replicate a simulation box of dimensions $L_x \times L_y \times L$ infinitely in x and y directions. This is achieved by the superposition property of the electrostatic potential, then the potential of the infinitely replicated ion is the sum of all potentials of each replica, resulting in

$$G(\boldsymbol{r};\boldsymbol{r}_0) = \frac{4q}{\epsilon L}\sum_{\boldsymbol{m}=-\infty}^{\infty}\sum_{n=1}^{\infty}\sin(k_n z)\sin(k_n z_0)K_0\left(k_n\sqrt{(x-x_0+m_xL_x)^2+(y-y_0+m_yL_y)^2}\right)\ , \tag{3.7}$$

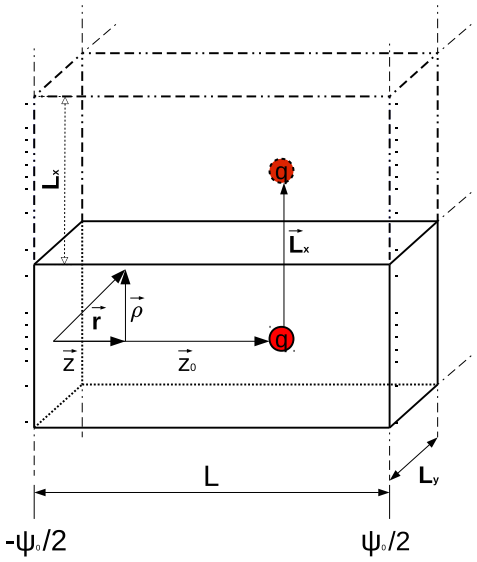

Figure 7: Point charge q located at $z_0\hat{\boldsymbol{z}}$ between two infinite metal electrodes with constant potential difference ψ_0. The electrodes are at $z = 0$ and $z = L$. The electrostatic potential is calculated at a point $\boldsymbol{r}$ indicated in cylindrical coordinates. The dashed lines show the first replica of the simulation box in the x direction.

where m's spam the integers, $(m_x, m_y) \in \mathbb{Z}$, ρ is now in Cartesian coordinates and $\boldsymbol{r}_0$ is the position of the particle in the main cell. The potential decays very rapidly in the x and y dimensions since the second-type Bessel function of order zero has an asymptotic behavior given by

$$K_0(x) \propto \sqrt{\frac{\pi}{2}}\frac{e^{-x}}{\sqrt{x}}[1 + \mathcal{O}(\frac{1}{x})] \qquad \text{as} \qquad x \to \infty \ . \tag{3.8}$$

Therefore, in Monte Carlo simulations, we need only a few replicas to achieved any desired accuracy. Unfortunately, we have a divergence when $\boldsymbol{m} = (0, 0)$, $x = x_0$ and $y = y_0$. This is due the $K_0(x)$ logarithmic divergence as $x \to 0$. However, physically, as long as $z \neq z_0$, the potential must remain finite, therefore the problem is purely mathematical: it is difficult to perform the limit correctly. Eq. 3.7 has a very low convergence rate for this specific condition. We, then, seek an alternative form for the Green function in order to avoid long and computationally expensive summations.

Once again we consider just *one* ion located at $\boldsymbol{r}_0$ between two grounded metallic surfaces. However, now we begin by expanding the Dirac delta in the coordinate ρ, consequently writing

$$\frac{1}{\rho}\delta(\rho) = \int_0^\infty kJ_0(k\rho)\mathrm{d}k \ , \tag{3.9}$$

where J_0 is the Bessel function of zeroth order. The electrostatic potential can now be written as

$$\phi(\rho, z; z_0) = \frac{q}{\epsilon}\int_0^\infty kJ_0(k\rho)g_k(z, z_0)\mathrm{d}k \ . \tag{3.10}$$

Substituting Eq. 3.10 into Eq. 3.1, we obtain an ordinary differential equation for $g_k(z, z_0)$:

$$\frac{\mathrm{d}^2 g_k}{\mathrm{d}z^2} - k^2 g_k = -2\delta(z - z_0) \ . \tag{3.11}$$

Applying the boundary conditions, we finally obtain

$$\phi(\rho, z; z_0) = \frac{q}{\epsilon} \int \mathrm{d}k J_0(k\rho) \frac{e^{k|z-z_0|-2kL} + e^{-k|z-z_0|} - e^{-k(z+z_0)} - e^{k(z+z_0)-2kL}}{1 - e^{-2kL}} \ , \tag{3.12}$$

which is well behaved when $\rho \to 0$, as long as $z \neq z_0$. This expression is equivalent to Eq. 4.4 and can be used to calculate the electrostatic potential produced by the ion inside the main simulation cell, replacing the $m_x = m_y = 0$ term of Eq. 3.7, since the integral will rapidly converge even if the function is to be calculated at $\rho = 0$.

Suppose an ion is placed at $z = z_0$ between two infinite grounded metal surfaces. How much charge will be induced on each electrode? The surface charge density on the left electrode is

$$\sigma(\rho) = -\frac{\epsilon}{4\pi} \frac{\partial \phi}{\partial z}\bigg|_{z=0} = -\frac{q}{2\pi} \int_0^\infty \mathrm{d}k J_0(k\rho) k \frac{\sinh[k(L - z_0)]}{\sinh(kL)} \ , \tag{3.13}$$

where we used the Green representation of Eq. 3.12. Now we perform an integration over all plate to obtain the *total* charge,

$$Q_l^0 = -\frac{q}{2\pi} \int \mathrm{d}\varphi \int \rho \mathrm{d}\rho \int \mathrm{d}k k J_0(k\rho) \frac{\sinh[k(L - z_0)]}{\sinh(kL)} \ . \tag{3.14}$$

Eq. 3.14 is conditionally convergent. To conveniently perform the integral we introduce a convergence factor $e^{-\alpha\rho}$ which allows us to change the order of integration. Performing the integration first over φ and ρ,

$$Q_l^0 = -q \int_0^\infty \mathrm{d}k \frac{k}{(1 + \frac{k^2}{\alpha^2})^{\frac{3}{2}} \alpha^2} \frac{\sinh[k(L - z_0)]}{\sinh(kL)} \ , \tag{3.15}$$

then changing variables $\frac{k}{\alpha} = a$ and taking the limit $\alpha \to 0$, we have

$$Q_l^0 = -q \int_0^\infty \mathrm{d}a \frac{a}{(1 + a^2)^{\frac{3}{2}}} (1 - z_0/L) \ , \tag{3.16}$$

which integrates to

$$Q_l^0 = -q(1 - \frac{z_0}{L}) \ . \tag{3.17}$$

Similarly the surface charge on the right electrode is $Q_r^0 = -qz_0/L$. So far our discussion has been restricted to the grounded metal surfaces. Nonetheless, often the electrostatic potential difference between the electrodes is controlled by an external battery. Thus we set the potential of the electrode located at $z = 0$ fixing it at $-\psi_0/2$ and of the electrode located at $z = L$ is fixed at $+\psi_0/2$. Using the uniqueness property of the Poisson equation, it is simple to account for the extra surface potential. The Uniqueness Theorem in electrostatics says that given a boundary

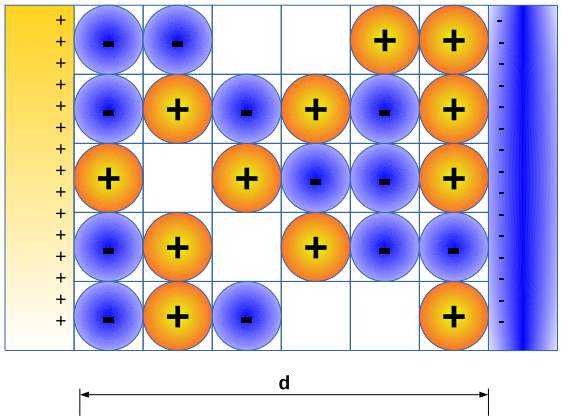

Figure 8: Lattice model of ionic liquid confined by electrified electrodes. The compacity parameter for this 2D example is $\gamma_d = \frac{5}{6}$.

condition, there is one and only one solution to the Laplace or Poisson equation. We observe that if we add to Eq. 3.7 a potential

$$\phi_s(z) = \left(\frac{z}{L} - \frac{1}{2}\right)\psi_0\,, \tag{3.18}$$

the sum will satisfy Eq. 3.1 with the appropriate new Dirichlet conditions. In addition, in simulations we replicate a charge neutral system with N ions at positions $\{\boldsymbol{r}_i\}$ and the electrodes are held at potentials $\mp\psi_0/2$, respectively. Thus using Eq. 3.17, discontinuity of electric field at the electrodes and superposition, the total charge on the left and right electrodes *within the simulation cell* will then be

$$Q_{l,r} = \mp\frac{\epsilon\psi_0 A}{4\pi L} \pm \sum_{i=1}^{N} q_i \frac{z_i}{L}\,, \tag{3.19}$$

where $A = L_x L_y$ is the area of the electrode inside the simulation cell. Note that $Q_l = -Q_r$.

We are now in a position to perform simulations of N-body Coulomb systems confined by two parallel metal electrodes.The object of particular interest for the room temperature ionic liquids community is the differential capacitance, which can be obtained from the fluctuations of the surface charge on the electrodes [57, 81]. The partition function in the fixed electrostatic potential ensemble is

$$\mathcal{Z}_\psi = \int \prod_{i=1}^{N} \mathrm{d}\boldsymbol{r}_i \int \mathrm{d}Q e^{-\beta[E(\boldsymbol{r}_1,\ldots,\boldsymbol{r}_N,Q)-\psi Q]}\,, \tag{3.20}$$

where $\beta = 1/k_B T$ and the surface charge on the left and right electrodes is $\mp Q$, respectively. Note that in this ensemble the surface charge on the electrodes is allowed to fluctuate. The differential capacitance of the system can then be calculated straightforwardly as

$$C = \frac{1}{A}\frac{\partial\langle Q\rangle}{\partial\psi} = \frac{1}{\beta A}\left(\frac{\partial^2 \ln \mathcal{Z}_\psi}{\partial\psi^2}\right) = \frac{\beta}{A}[\langle Q^2\rangle - \langle Q\rangle^2]\,. \tag{3.21}$$

It is important to note that in order to perform a simulation at a *fixed electrostatic potential*,

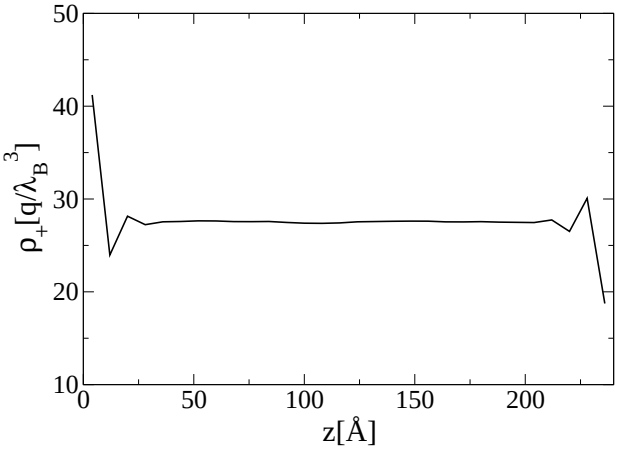

Figure 9: Cationic profile of ionic liquid between the electrodes. The parameters are: $\gamma_d = \frac{1}{2}$, $\lambda_B = 38.4\text{Å}$ and $\psi = 0.05V$.

we need to know the total electrostatic energy $E(Q)$ of a system with electrodes carrying a *fixed amount* of surface charge $-Q$ and $+Q$, respectively. Since the electrodes are metallic, they must be equipotential. This means that the distribution of the surface charge will *not* be uniform and will respond to ionic motion. For a given Q, the surface potential ψ_0 will, therefore, fluctuate. Instead, the *external* potential ψ is fixed in the simulations and determined by the source battery. The two potentials differ in the sense that ψ_0 is used to satisfy Neumann and Dirichlet conditions. Note that if $\psi = \psi_0$ the derivative on Eq. 3.21 would not calculate the differential capacitance. Since the system is charge neutral, the surface potential for a given ionic distribution inside the simulation cell can be easily calculated using Eq. 3.19,

$$\psi_0 = \frac{4\pi L}{\epsilon A}\left(Q + \sum_{i=1}^{N} q_i \frac{z_i}{L}\right). \tag{3.22}$$

The total electrostatic energy inside the simulation cell is then

$$E(Q) = \frac{1}{2}\sum_{i\neq j}^{N} q_i G(\boldsymbol{r}_i;\boldsymbol{r}_j) + \sum_{i=1}^{N}\left[U_s(\boldsymbol{r}_i) + \frac{1}{2}q_i\phi_s(z_i)\right] + \frac{1}{2}\psi_0 Q, \tag{3.23}$$

where the periodic Green function is given by Eq. 3.7 with $m_x = m_y = 0$ term replaced by Eq. 3.12, and the self energy of an ion at $\boldsymbol{r}_i$ is

$$U_s(\boldsymbol{r}_i) = \frac{q_i}{2}\lim_{\rho\to 0}\left[G(\boldsymbol{r}_i;\boldsymbol{r}_i) - \frac{q_i}{\epsilon\rho}\right]. \tag{3.24}$$

The self energy corresponds to the work necessary to bring an ion from the bulk to the confinement. Alternatively, is the energy to bring the metal plates from the infinity to their distance L, with the confined charge. Using the identity

$$\int_0^\infty \mathrm{d}k J_0(k\rho) = \frac{1}{\rho}, \tag{3.25}$$

the limit in Eq. 3.24 can be performed explicitly [82], resulting in

$$U_s(\boldsymbol{r}_i) = \frac{q^2}{2\epsilon}\int \mathrm{d}k \frac{2e^{-2kL} - e^{-2kz_i} - e^{2kz_i - 2kL}}{1 - e^{-2kL}} + \frac{2q^2}{\epsilon L}\sum_{\boldsymbol{m}\neq\boldsymbol{0}}\sum_{n=1}^{\infty}\sin^2(k_n z_i) K_0\left(k_n\sqrt{m_x^2 L_x^2 + m_y^2 L_y^2}\right) \ . \tag{3.26}$$

We reinforce that the rapid decay of modified Bessel function of second-type allows one to perform the summation of just a few replicas to achieve an accuracy of double-precision variable in energy. To demonstrate the utility of the present method we study a Coulomb lattice gas [24, 83–86] confined between two electrodes held at potential $\mp\psi/2$, respectively. The system is depicted in Fig. 8. The simulations are made fast by precalculating the potential at each site, thus this technique might be used for studying more complicated configurations which are not accessible in continuum simulations. Examples are: asymmetry in charge and in size of the ions, high coupling parameters and large volume fractions. We use Metropolis algorithm [5] to sample in accordance with Eq. 3.20. Movements are between charged ions and between charged ions and empty sites, in which the electrode charge remains constant and the energy difference is calculated using Eq. 3.23. Also, the electrode charge can change as a trial move, and each configuration is accessed with probability proportional to the Boltzmann weight.

The simulations are performed in a cell of volume $V = L_x L_y L$, with $L_x = L_y = 80\text{Å}$ and $L = 3L_x$. The lattice gas is confined in the region $-L_x/2 < x < L_x/2$, $-L_y/2 < y < L_y/2$ and $0 < z < L$. The negatively charged electrode is positioned at $z = 0$ and the positive one at $z = L$. We define the Bjerrum length as $\lambda_B = q^2/k_B T\epsilon$, and consider two specific values $\lambda_B = 7.2\text{Å}$ and $\lambda_B = 38.4\text{Å}$. The first value is appropriate for room temperature electrolytes while the the second is for room temperature ionic liquids [87–89], which have dielectric constant around $\epsilon = 15$. The concentration of ionic liquid is controlled by the compacity factor $\gamma_d = (N_+ + N_-)/(N_+ + N_- + N_0)$, where N_+ is the number of cations, N_- the number of anions, and N_0 the number of voids. We will set γ_d to $\frac{1}{20}$ for electrolytes, and $\frac{1}{2}$ for ionic liquids. The lattice spacing is set to 8Å, characteristic of ionic diameter. For now we consider a symmetric case with charge of cation q and charge of anions $-q$, where q is the charge of the proton. The model, however, can be easily extended to asymmetric ionic liquids. In the simulations we have used around $\approx 10^4$ $\boldsymbol{m}$-vectors in the energy computation. The averages were calculated with 5×10^4 uncorrelated samples after equilibrium was achieved.

In Fig. 9 we show the oscillatory behavior of the counterion density profile near an electrode [19], which is signature of such strongly correlated systems. Fig. 10 (a) shows the characteristic minimum of differential capacitance at zero potential predicted by the Poisson-Boltzmann theory, followed by a maximum for higher applied voltages. The behavior is characteristic of electrolyte solutions [90] and is qualitatively measured in experiments. On the other hand, in the regime of ionic liquids where steric and electrostatic correlations play the dominant role [39], the behavior is

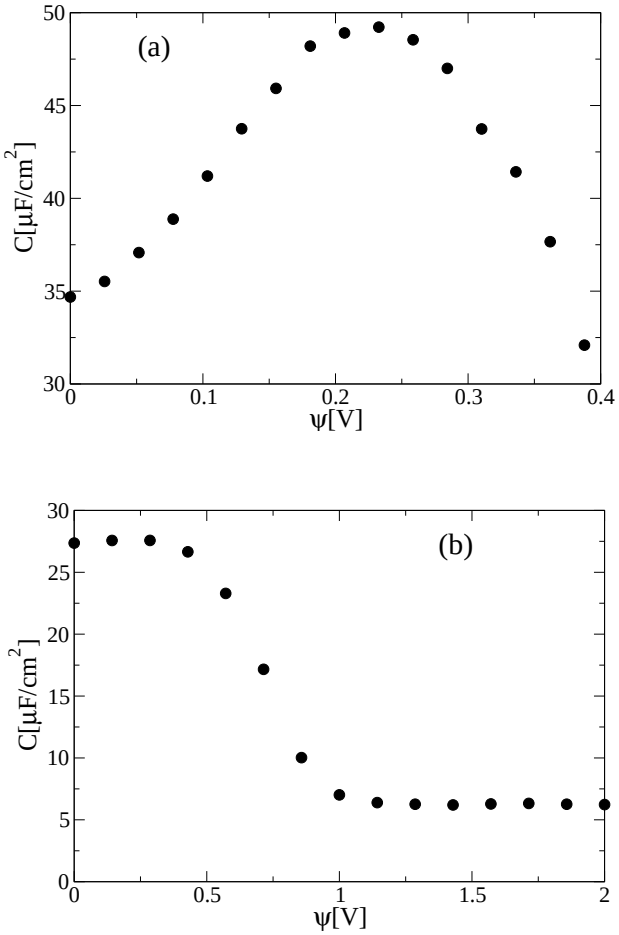

Figure 10: Differential capacitance calculated using Eq. 3.21. Panel (a) shows the electrolyte regime with parameters $\gamma_d = \frac{1}{20}$ and $\lambda_B = 7.2$Å; and (b) shows the typical bell-shaped differential capacitance of ionic liquids, $\gamma_d = \frac{1}{2}$ and $\lambda_B = 38.4$Å.

quite different [91,92]. Fig. 10 (b) shows that unlike electrolytes, ionic liquids have a maximum of differential capacitance at $\psi = 0$V. It is gratifying to see that a simple lattice model captures this complicated transition of differential capacitance between electrolyte and ionic liquid regimes.

4 Ionic liquids confined by general polarizable surfaces

In this chapter we consider general polarizable surfaces confining charged fluids. We begin by considering a point particle of charge q_i at position $\mathbf{r}_i = (x_i, y_i, z_i)$ inside a simulation box with sides of lengths L_x, L_y, and L; in x, y, and z directions, respectively. This system is replicated

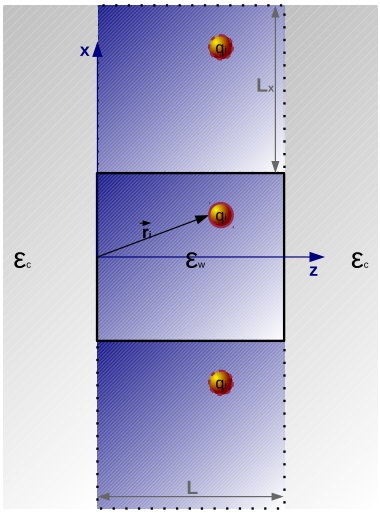

Figure 11: Representation of the confined system. The walls are polarizable. Only the first two replicas in $\hat{\boldsymbol{x}}$ of the simulation cell are shown.

along the x and y axis, generating an infinite periodic charged system of finite width L in the z direction. The dielectric constant in the region $0 < z < L$ is ϵ_w, while in the regions $z < 0$ and $z > L$ it is ϵ_c, see Fig. 11. Afterwards, the results will be generalized for three different dielectric constants. The electrostatic potential at position $\mathbf{r} = (x, y, z)$ satisfies the Poisson equation

$$\nabla^2 G(\mathbf{r}, \mathbf{r}_i) = -\frac{4\pi q_i}{\epsilon_w} \sum_{m_x, m_y = -\infty}^{\infty} \delta(\boldsymbol{r} - \boldsymbol{r}_i + m_x L_x \hat{\boldsymbol{x}} + m_y L_y \hat{\boldsymbol{y}}) \ . \tag{4.1}$$

The periodic delta function can be expressed using Fourier transform representation as

$$\sum_{m_x, m_y = -\infty}^{\infty} \delta(x - x_i + m_x L_x)\delta(y - y_i + m_y L_y) = \frac{1}{L_x L_y} \sum_{\boldsymbol{m} = -\infty}^{\infty} e^{i\left[\frac{2\pi m_x}{L_x}(x - x_i) + \frac{2\pi m_y}{L_y}(y - y_i)\right]} \ , \tag{4.2}$$

where $\boldsymbol{m} = (m_x, m_y)$. We now write the Green function as

$$G(\mathbf{r}, \mathbf{r}_i) = \frac{1}{L_x L_y} \sum_{\boldsymbol{m} = -\infty}^{\infty} g_{\boldsymbol{m}}(z_i, z) e^{i\left[\frac{2\pi m_x}{L_x}(x - x_i) + \frac{2\pi m_y}{L_y}(y - y_i)\right]} \ , \tag{4.3}$$

which is periodic in $\hat{\boldsymbol{x}}$ and $\hat{\boldsymbol{y}}$ directions. Inserting Eq. 4.3 into Eq. 4.1 we obtain

$$\frac{\partial^2 g_{\boldsymbol{m}}(z_i, z)}{\partial z^2} - k^2 g_{\boldsymbol{m}}(z_i, z) = -\frac{4\pi q_i}{\epsilon_w} \delta(z - z_i) \ , \tag{4.4}$$

where $k = 2\pi\sqrt{m_x^2/L_x^2 + m_y^2/L_y^2}$. The general solution of Eq. 4.4 has the form $Ae^{-kz} + Be^{kz}$. The electrostatic potential must vanish as $z \to \pm\infty$, restricting its form in the outer regions, $z < 0$ and $z > L$, to a decaying exponential. The others boundary conditions are the continuity of potential and discontinuity of displacement vector at the walls. In order to account for the singularity of the delta function, we use the symmetry property of Green function, $g_{\boldsymbol{m}}(z_i, z) = g_{\boldsymbol{m}}(z, z_i)$. Thus, we have the solution to the Neumann and Dirichlet boundary conditions problem written as

$$g_{\boldsymbol{m}}(z_i, z) = \frac{2\pi q_i}{\epsilon_w k(1-\gamma^2 e^{-2kL})} \times \left[e^{-k|z-z_i|} + \gamma e^{-k(z+z_i)} + \gamma e^{-2kL} e^{k(z+z_i)} + \gamma^2 e^{-2kL} e^{k|z-z_i|}\right] , \tag{4.5}$$

where $\gamma = (\epsilon_w - \epsilon_c)/(\epsilon_w + \epsilon_c)$. As the surviving terms in the $\boldsymbol{m}$ summation are just the cosine functions, the potential assumes the form

$$G(\mathbf{r}, \mathbf{r}_i) = \frac{1}{L_x L_y} \sum_{\boldsymbol{m}} g_{\boldsymbol{m}}(z_i, z) \cos\left[\frac{2\pi m_x}{L_x}(x - x_i) + \frac{2\pi m_y}{L_y}(y - y_i)\right] . \tag{4.6}$$

In the absence of dielectric contrast, $\gamma \to 0$, Eq. 4.6 reduces to

$$G_0(\mathbf{r}, \mathbf{r}_i) = \frac{2\pi q_i}{\epsilon_w L_x L_y} \sum_{\boldsymbol{m}=-\infty}^{\infty} \frac{e^{-k|z-z_i|}}{k} \cos\left[\frac{2\pi m_x}{L_x}(x - x_i) + \frac{2\pi m_y}{L_y}(y - y_i)\right] , \tag{4.7}$$

which is a representation of the electrostatic potential produced by a periodically replicated point charge in the x and y directions. Eq. 4.7 diverges in the limit $k \to 0$, when m_x,$m_y \to 0$. Although this divergence can be renormalized, the remaining sum is still slowly convergent. We note, however, that the electrostatic potential described by Eq. 4.7 can be efficiently calculated using a modified 3d Ewald Summation technique [40, 45] or other other methods [17, 63]. The details of the 3d Ewald Summation are presented in the first Chapter of this Thesis. With the aid of Eq. 4.7 we can rewrite the total electrostatic potential as

$$G(\mathbf{r}, \mathbf{r}_i) = [G(\mathbf{r}, \mathbf{r}_i) - G_0(\mathbf{r}, \mathbf{r}_i)] + G_0(\mathbf{r}, \mathbf{r}_i) . \tag{4.8}$$

We define $\tilde{G}(\mathbf{r}, \mathbf{r}_i) = G(\mathbf{r}, \mathbf{r}_i) - G_0(\mathbf{r}, \mathbf{r}_i)$ as the polarization contribution to the total Green function given by

$$\begin{aligned}\tilde{G}(\mathbf{r}, \mathbf{r}_i) =& \frac{2\pi q_i}{\epsilon_w L_x L_y} \sum_{\boldsymbol{m}=-\infty}^{\infty} \frac{1}{k(1-\gamma^2 e^{-2kL})} \left[\gamma e^{-k(z+z_i)} + \gamma e^{-2kL} e^{k(z+z_i)} + 2\gamma^2 e^{-2kL} \cosh\left(k(z - z_i)\right)\right] \times \\ & \cos\left[\frac{2\pi m_x}{L_x}(x - x_i) + \frac{2\pi m_y}{L_y}(y - y_i)\right] .\end{aligned} \tag{4.9}$$

The limit $k \to 0$, $m_x = m_y = 0$, requires additional care. Once again renormalization procedures are necessary. We split the calculations for three cases: $\gamma = +1$, $\gamma = -1$ and $\gamma \in (-1, 1)$. For $-1 < \gamma < 1$ we find that the $m_x = m_y = 0$ term diverges as

$$-\frac{4\pi q_i}{\epsilon_w L_x L_y}\left[\frac{\gamma}{k(\gamma - 1)} + \frac{\gamma L}{(\gamma - 1)^2} + \mathcal{O}(k)\right] . \tag{4.10}$$

Since this is a constant, position *independent*, it will not contribute to the force and can be renormalized away. For $\gamma = -1$, we find that $m_x = m_y = 0$ term contains an infinite constant and a finite function of z,

$$\frac{2\pi q_i}{\epsilon_w L_x L_y}\left[-\frac{1}{k} + (z + z_i - 2\frac{z_i z}{L}) + \mathcal{O}(k)\right] \ . \tag{4.11}$$

Once again neglecting the infinite constant, we write

$$G_{(-1)}(\mathbf{r}, \mathbf{r}_i) = \frac{2\pi q_i}{\epsilon_w L_x L_y}(z + z_i - 2\frac{z_i z}{L}) \ . \tag{4.12}$$

For $\gamma = 1$ we find

$$\frac{2\pi q_i}{\epsilon_w L_x L_y}\left[\frac{2}{Lk^2} - \frac{1}{k} + \frac{2L^2 - 3L(z + z_i) + 3(z^2 + z_i^2)}{3L} + \mathcal{O}(k)\right] \ , \tag{4.13}$$

so that

$$G_{(+1)}(\mathbf{r}, \mathbf{r}_i) = \frac{2\pi q_i}{\epsilon_w L_x L_y}\left[-(z + z_i) + \frac{z^2 + z_i^2}{L}\right] \ . \tag{4.14}$$

Now we are able to properly write the potential in a fashion where it is evident the contribution of the polarized walls. Furthermore, the polarization "portion" is decoupled of periodic ionic contribution. The final expression for the total electrostatic potential can now be written as

$$G(\mathbf{r}, \mathbf{r}_i) = G_0(\mathbf{r}, \mathbf{r}_i) + G_{(\gamma)}(\mathbf{r}, \mathbf{r}_i) + \frac{2\pi q_i}{\epsilon_w L_x L_y} \sum_{\boldsymbol{m}'=-\infty}^{\infty} \frac{1}{k(1 - \gamma^2 e^{-2kL})} \times$$
$$\left(\gamma e^{-k(z+z_i)} + \gamma e^{-2kL} e^{k(z+z_i)} + 2\gamma^2 e^{-2kL} \cosh\left(k|z - z_i|\right)\right) \cos\left[2\pi(\frac{m_x}{L_x}(x - x_i) + \frac{m_y}{L_y}(y - y_i))\right] \ , \tag{4.15}$$

where the function $G_{(\gamma)}(\mathbf{r}, \mathbf{r}_i)$ is non-zero only for $\gamma = +1$ and -1 and the prime excludes $m_x = m_y = 0$ term in the summation.

The total energy for a system of N periodically replicated charged particles is then given by

$$U = \frac{1}{2}\sum_{i=1}^{N}\sum_{j=1}^{N} q_j G(\mathbf{r}_j, \mathbf{r}_i) \ . \tag{4.16}$$

We can split the total energy into the polarization and direct Coulomb contributions

$$U = U_{Ew} + U_p \ , \tag{4.17}$$

where U_{Ew} is the direct Coulomb contribution,

$$U_{Ew} = \sum_{i=1}^{N}\sum_{j=1}^{N} q_j \frac{G_0(\mathbf{r}_j, \mathbf{r}_i)}{2} \ , \tag{4.18}$$

which can be calculated using the modified 3d Ewald Summation method, see first Chapter.

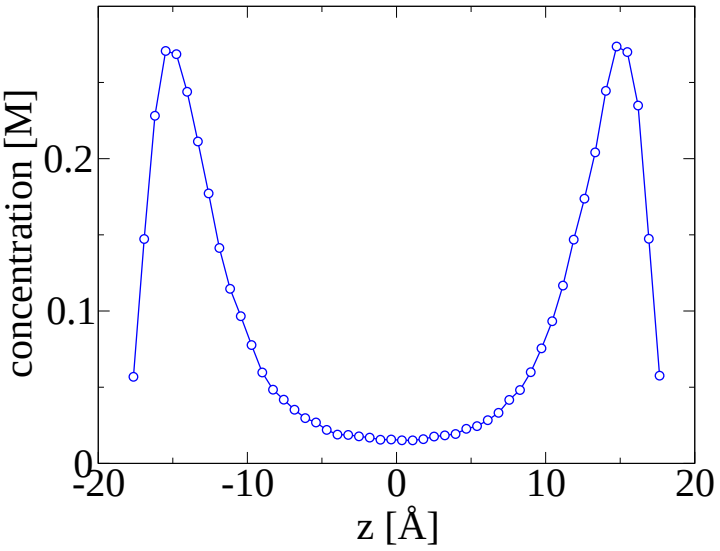

Figure 12: Density profile of trivalent counterions confined between charged dielectric surfaces, $\gamma = 0.95$. The surfaces charge densities are -0.05 C/m^2. The line is a guide to the eyes.

Here we point that this separation is seminal to the possible relevance of the algorithm. Taking advantage of this property of the Green function, we can account for general polarizable walls while using *others* already well-established methods for 2d+h geometry. The energy U_p due to surface polarizability can be rewritten as

$$U_p = U_\gamma + \frac{\pi}{\epsilon_w L_d^2} \sum_{\boldsymbol{m}'} \frac{\gamma}{k(1-\gamma^2 e^{-2kL})} \times \{f_1(\boldsymbol{m})^2 + f_2(\boldsymbol{m})^2 + e^{-2kL}\left(f_3(\boldsymbol{m})^2 + f_4(\boldsymbol{m})^2\right) + 2\gamma e^{-2kL}[f_3(\boldsymbol{m})f_1(\boldsymbol{m}) + f_2(\boldsymbol{m})f_4(\boldsymbol{m})]\} \ , \tag{4.19}$$

where without loss of generality we have set $L_x = L_y = L_d$. The number of integers, (m_x, m_y), necessary to obtain a converged energy will depend on the lateral size of the simulation box, L_d. The contribution U_γ arises from the $k \to 0$ limit, and is zero if $\gamma \in (-1, 1)$. For $\gamma = -1$ we find

$$U_{(-1)} = -\frac{2\pi}{L_d^2}\left[\frac{M_z^2}{L} - Q_t M_z\right] \ , \tag{4.20}$$

where $Q_t = \sum_{i=1}^N q_i$ and $M_z = \sum_{i=1}^N q_i z_i$. For $\gamma = +1$ we obtain

$$U_{(+1)} = -\frac{2\pi Q_t}{L_d^2}\left[M_z - \frac{\Omega_z}{L}\right] \ , \tag{4.21}$$

where $\Omega_z = \sum_{i=1}^N q_i z_i^2$. The $f_i(\boldsymbol{m})$ functions are defined as

$$f_1(\boldsymbol{m}) = \sum_{i=1}^N q_i \cos\left[\frac{2\pi}{L_d}(m_x x_i + m_y y_i)\right] e^{-kz_i} \ , \tag{4.22}$$

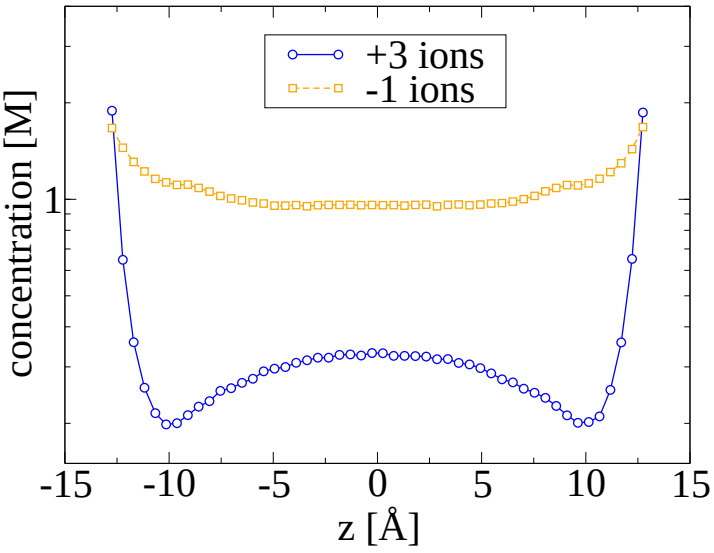

Figure 13: Density profiles of cations and anions confined between grounded metal surfaces, $\gamma = -1$. The $3:1$ salt concentration is 0.35 M. The lines are guides to the eye.

$$f_2(\boldsymbol{m}) = \sum_{i=1}^{N} q_i \sin\left[\frac{2\pi}{L_d}(m_x x_i + m_y y_i)\right] e^{-kz_i} \ , \tag{4.23}$$

$$f_3(\boldsymbol{m}) = \sum_{i=1}^{N} q_i \cos\left[\frac{2\pi}{L_d}(m_x x_i + m_y y_i)\right] e^{kz_i} \ , \tag{4.24}$$

$$f_4(\boldsymbol{m}) = \sum_{i=1}^{N} q_i \sin\left[\frac{2\pi}{L_d}(m_x x_i + m_y y_i)\right] e^{kz_i} \ . \tag{4.25}$$

Note that k depends on $\boldsymbol{m}$ and the f functions must be updated for each particle move. There is, however, no need to recalculate all the functions, but only the contribution to each function that depends on the position of the particle that is being moved. This makes the energy update very efficient in Monte Carlo simulations. Finally, if there is a surface charge present at the interfaces, it can be included as an external potential, see Ref. [45],

$$U_{sur} = -\frac{2\pi(\sigma_1 - \sigma_2)}{\epsilon_w} \sum_{i=1}^{N} q_i z_i \ , \tag{4.26}$$

where σ_1 and σ_2 are the surface charge densities at $z = 0$ and $z = L$, respectively.

To demonstrate the utility of the new simulation method, we perform Monte Carlo simulations of an charged solution in the NVT ensemble using Metropolis algorithm [5]. To efficiently sample the phase space we use both short and long displacement moves [3, 10]. The effective ionic radii are set to $r_c = 2$ Å. The Bjerrum length, defined as $q^2\beta/\epsilon_w$, where β is the inverse thermal energy and q is the proton charge, is set to 7.2 Å, typical value for water at room temperature. The

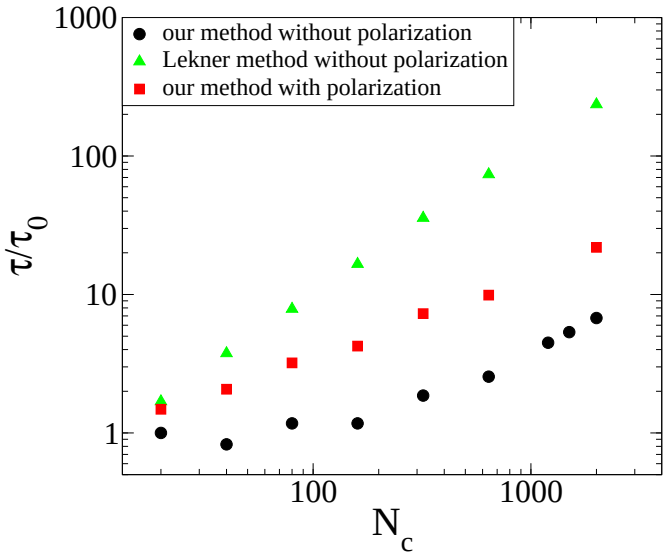

Figure 14: CPU time to perform 10^6 energy updates as a function of the number of particles in the system. The distance between the polarizable plates is $L = 10$Å, with $\gamma = 0.95$. The Bjerrum length was set to $\lambda_B = 14.5$Å, the superficial charge to $\sigma = -0.12\text{C/m}^2$ and ionic radius to 2Å. τ_0 is the CPU time to perform 10^6 energy updates.

system relaxes to equilibrium in 1×10^6 Monte Carlo steps. The ionic density profiles are obtained using 1×10^5 uncorrelated samples.

In Fig. 12 we show the density profile of trivalent counterions confined between charged dielectric surfaces of $\gamma = 0.95$. The confining surfaces are separated by a distance $L = 40$ Å. The number of counterions is $N_c = 100$ and the surfaces are equally charged with charge density -0.05 C/m^2. We see a strong repulsion of ions from the interface produced by the induced surface charge. This result is in agreement with an earlier image charge algorithm [28]. However, the present method is an order of magnitude more efficient.

In Fig. 13 we show the density profiles of cations and anions of a dissolved 3:1 electrolyte at concentration 0.35 M, confined by grounded metal electrodes, $\gamma = -1$, separated by distance $L = 30$ Å.Now, instead of the repulsion of the previous case, we see the expected attraction of charges to the metal electrodes. This effect can be understood considering the image charges of opposite sign induced inside the electrodes.

Finally, in Fig. 14 we compare the characteristic central processing unit (CPU) times of our simulation method with a standard implementation of Lekner Summation which does not account for polarization [17]. We see that for reasonably large system sizes, Lekner Summation is at least an order of magnitude slower than our method. Furthermore, for large N_c we see that even for systems with polarization our method remains an order of magnitude faster than Lekner

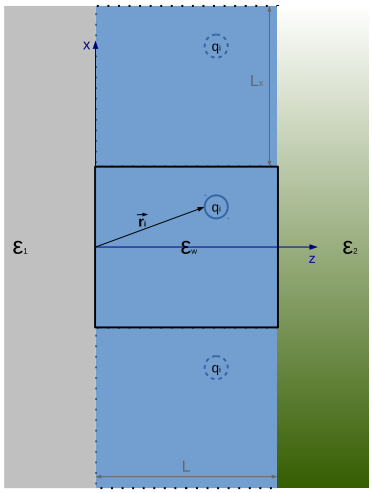

Figure 15: Representation of the confined system. The walls are polarizable. Only the first two replicas in $\hat{\boldsymbol{x}}$ direction of the simulation cell are shown.

Summation without polarization.

Seeking completeness, we write down the energy for a periodic system of N particles confined between surfaces with *different* dielectric discontinuities. The system is depicted in Fig. 15. The algorithm to obtain the equation is the same as described above and the polarization energy is also decoupled from the ion-ion interaction. Nonetheless, there will be a position *dependent* renormalization term for $\gamma_1, \gamma_2 \in [-1, 1]$. We note that if $\gamma_1 = \gamma_2 = \mp 1$ the U_γ term is already calculated. Finally we have

$$U_p = U_\gamma + \frac{\pi}{L_d^2 \epsilon_w} \sum_{\boldsymbol{m}\neq 0} \frac{1}{k(1-\gamma_1\gamma_2 e^{-2kL})} \times$$
$$\{\gamma_1 (f_1(\boldsymbol{m})^2 + f_2(\boldsymbol{m})^2) + e^{-2kL}\gamma_2 \left(f_3(\boldsymbol{m})^2 + f_4(\boldsymbol{m})^2\right) + 2\gamma_1\gamma_2 e^{-2kL}[f_3(\boldsymbol{m}) f_1(\boldsymbol{m}) + f_2(\boldsymbol{m}) f_4(\boldsymbol{m})]\} \ , \tag{4.27}$$

where U_γ arises from the term $\boldsymbol{m} = \boldsymbol{0}$ and assumes the shape

$$U_\gamma = \frac{2\pi Q_t M_z}{L_d^2 \epsilon_w} \frac{\gamma_1 - \gamma_2}{1 - \gamma_1\gamma_2} \ . \tag{4.28}$$

As required, for $\gamma_1 = \gamma_2 = \gamma$ all equations reduce to known results.

5 Conclusions

In this Thesis we derived algorithms to computer simulate confined charged fluids in a *quasi* bi-dimensional geometry. We first showed a care full deduction of 3d Ewald Summation for bulk systems, with special attention to the $\boldsymbol{k} = \mathbf{0}$ term. This term, though discussed in literature, lacked a proper formal mathematical analyzes. We showed that, contrary to Yeh and Berkowitz, there are geometry dependent terms even for bulk systems. However, on practice, this term seems to have no effect on the averaging over the canonical function. Then we took the limit of bulk to slab geometry and calculated the energy formulæ to perform simulations. We were able to gain considerable computational time when we treated charged walls as external linear potentials. This was possible because the transverse fields of the replicated plates cancel out in the main simulation box, remaining just a simple linear term for the interaction ion-plates. Also, our formalism can handle non-neutral systems. We point that our method can be made faster by adopting Particle-Particle Particle-Mesh approaches [11, 12, 14, 15].

We then have presented a new method to simulate charged systems confined by metal electrodes. Our algorithm was constructed using periodic Green functions. Also, the potential in the periodic dimensions was screened by the induced charges at the walls, allowing the use of just a few replicas for Monte Carlo simulations. The main advantage of the method is that to calculate the induced charges at boundaries a simple linear equation must be solved, in contrast with very computationally expensive methods of energy minimizations. As a demonstration of the utility of the recipe we applied it for electrolytes and room temperature ionic liquids, considering a Coulombic lattice gas. Our simple model captured the complex transition of the capacitance shape that is a signature of such systems. In future work we will apply this method with the support of optimal sampling methods, like parallel-tempering [93] or generalized cluster algorithms [94], to simulate ionic liquids in the continuum limit.

Finally, we have presented an efficient new method for simulating Coulomb systems confined by general polarizable walls. We solved the Poisson Equation with the periodic eigenfunctions of the Laplace operator. The result was a periodic Green function for the potential of the system. We showed that we can split the energy into contributions due to direct Coulomb interactions and due to polarization effects. The former can be computed using already developed methods, specially the one shown in previous Chapter. The latter was written in a conventional shape so each Monte Carlo trial movement is cheap computationally speaking. This way, a recalculation of all the energetic contribution at each step is avoided, demonstrating the rapid characteristic of our method. The results of the new simulation method was compared to previous approaches [28, 74] and lead to exactly same results. Finally, we noted that our calculations are easily extended for

systems with three dielectric media.

References

[1] O K Rice. On The Statistical Mechanics of Liquids. *J. Chem. Phys.*, 12:1–18, 1944.

[2] J K Bernal. The Bakerian Lecture, 1962: The Structure of Liquids. *Proc. R. Soc.*, 280:299–322, 1964.

[3] Frenkel D. and Smit, B. *Understanding Molecular Simulation.* Academic, San Diego, United States of America, 2002.

[4] G Dyson. *Turing's Cathedral.* Vintage Books, New York, United States of America, 2012.

[5] N Metropolis, A W Rosenbluth, M N Rosenbluth, A H Teller, and E Teller. Equation of State Calculations by Fast Computing Machines. *J. Chem. Phys.*, 21:1087–1092, 1953.

[6] E Fermi, J Pasta, and S Ulam. Studies of Nonlinear Problems. I. *Los Alamos Sci. Rep.*, 630:1–20, 1955.

[7] A Rahman. Correlations in the Motion of Atoms in Liquid Argon. *Phys. Rev.*, 136:A405–A411, 1964.

[8] A P dos Santos, M Girotto, and Y Levin. Simulations of Coulomb Systems with Slab Geometry Using an Efficient 3D Ewald Summation Method. *J. Chem. Phys.*, 144:144103–144109, 2016.

[9] P Ewald. Die Berechnung Optischer und Elektrostatischer Gitterpotentiale. *Ann. Phys.*, 369:253–287, 1921.

[10] Allen, M. P. and Tildesley, D. J. *Computer Simulations of Liquids.* Oxford: Oxford University Press, New York, United States of America, 1987.

[11] U Essmann, L Perera, M L Berkowitz, T Darden, H Lee, and L G Pedersen. A Smooth Particle Mesh Ewald Method. *J. Chem. Phys.*, 103:8577–8593, 1995.

[12] T Darden, D York, and L Pedersen. Particle Mesh Ewald: An $N\dot{\log}(N)$ Method for Ewald Sums in Large Systems. *J. Chem. Phys.*, 98:10089–10092, 1993.

[13] J Kolafa and J W Perram. Cutoff Errors in the Ewald Summation Formulae for Point Charge Systems. *Mol. Simul.*, 9:351–368, 1992.

[14] M Deserno and C Holm. How to Mesh Up Ewald Sums. I. An Accurate Error Estimate for the Particle-Particle-Particle-Mesh Algorithm. *J. Chem. Phys.*, 109:7678–7693, 1998.

[15] M Deserno and C Holm. How to Mesh Up Ewald Sums. II. An Accurate Error Estimate for the Particle-Particle-Particle-Mesh Algorithm. *J. Chem. Phys.*, 109:7694–7701, 1998.

[16] Z Hu. Infinite Boundary Terms of Ewald Sums and Pairwise Interactions for Electrostatics in Bulk and at Interfaces. *J. Chem. Theory Comput.*, 10:5254–5264, 2014.

[17] J Lekner. Summation of Coulomb Fields in Computer-Simulated Disordered Systems. *Physica A*, 176:485–498, 1991.

[18] A H Widmann and D B Adolf. A Comparison of Ewald Summation Techniques for Planar Surfaces. *Comput. Phys. Commun.*, 107:167–186, 1997.

[19] M V Fedorov and A A Kornishev. Ionic Liquids at Electrified Interfaces. *Chem. Rev.*, 114:2978–3036, 2014.

[20] S Reed, O Lanning, and P Madden. Electrochemical Interface between an Ionic Liquid and a Model Metallic Electrode. *J. Chem. Phys.*, 126:084704, 2007.

[21] C Lian, K Liu, K L Van Aken, Y Gogotsi, D J Wesolowski, H L Liu, D E Jiang, and J Z Wu. Enhancing the Capacitive Performance of Electric Double-Layer Capacitors with Ionic Liquid Mixtures. *ACS Energy Lett.*, 1:21–26, 2016.

[22] M Dudka, S Kondrat, A Kornyshev, and G Oshanin. Phase Behavior and Structure of a Superionic Liquid in Nonpolarized Nanoconfinement. *J. Phys.: Condens. Matt.*, 28:466007, 2016.

[23] S Coles, M Mishin, S Perkin, M Fedorov, and V Ivanistsev. The Nanostructure of a Lithium Glyme Solvate Ionic Liquid at Electrified Interfaces. *Phys. Chem. Chem. Phys.*, 19:11004–11010, 2017.

[24] M Girotto, T Colla, A dos Santos, and Y Levin. Lattice Model of an Ionic Liquid at an Electrified Interface. *J. Phys. Chem. B*, 121:6408–6415, 2017.

[25] C Wong and M Muthukumar. Polymer Capture by Electro-Osmotic Flow of Oppositely Charged Nanopores. *J. Chem. Phys.*, 126:164903–164905, 2007.

[26] P Cazade, R Hartkamp, and B Coasne. Structure and Dynamics of an Electrolyte Confined in Charged Nanopores. *J. Phys. Chem. C*, 118:5061–5072, 2014.

[27] S Kondrat, N Georgi, M Fedorov, and A Kornyshev. A Superionic State in Nano-Porous Double-Layer Capacitors: Insights from Monte Carlo Simulations. *Phys. Chem. Chem. Phys.*, 13:11359–11366, 2013.

[28] A P dos Santos and Y Levin. Electrolytes between Dielectric Charged Surfaces: Simulations and Theory. *J. Chem. Phys.*, 142:194104, 2015.

[29] T Colla, M Girotto, A P dos Santos, and Y Levin. Charge Neutrality Breakdown in Confined Aqueous Electrolytes: Theory and Simulation. *J. Chem. Phys.*, 145:094704, 2016.

[30] Z Luo, Y Xing, Y Ling, A Kleinhammes, and Y Wu. Electroneutrality Breakdown and Specific Ion Effects in Nanoconfined Aqueous Electrolytes Observed by NMR. *Nat. Commun.*, 6:6358–6365, 2015.

[31] L Šamaj and E Trizac. Counterions at Highly Charged Interfaces: From One Plate to Like-Charge Attraction. *Phys. Rev. Lett.*, 106:078301, 2011.

[32] P Linse and V Lobaskin. Electrostatic Attraction and Phase Separation of Like-Charged Colloidal Particles. *Phys. Rev. Lett.*, 83:4208–4211, 1999.

[33] M Hatlo and L Lue. Electrostatic Interactions of Charged Bodies from The Weak-to-The-Strong-Coupling Regime. *Euro. Phys. Lett.*, 89:25002, 2010.

[34] R Netz and H Orland. Beyond Poisson-Boltzmann: Fluctuation Effects and Correlation Functions. *The Euro. Phys. Journ. E*, 1:203–214, 2000.

[35] Y Levin. When Do Like Charges Attrack? *Physica A*, 265:432–439, 1999.

[36] Alberto Martin-Molina, Jose Guadalupe Ibarra-Armenta, Enrique Gonzalez-Tovar, Roque Hidalgo-Alvarez, and Manuel Quesada-Perez. Monte Carlo Simulations of The Electrical Double Layer Forces in The Presence of Divalent Electrolyte Solutions: Effect of The Ion Size. *Soft Matter*, 7:1441–1449, 2011.

[37] A Grosberg, T Nguyen, and B Shklovskii. Colloquium: The Physics of Charge Inversion in Chemical and Biological Systems. *Rev. Mod. Phys.*, 329:329–345, 2002.

[38] Z Wang and J Wu. Ion Association at Discretly-Charged Dielectric Interfaces: Giant Charge Inversion. *J. Chem. Phys.*, 147:024703, 2017.

[39] Y Levin. Electrostatic Correlations: from Plasma to Biology. *Rep. Prog. Phys.*, 65:1577, 2002.

[40] I C Yeh and M L Berkowitz. Ewald Summation for Systems with Slab Geometry. *J. Chem. Phys.*, 111:3155–3162, 1999.

[41] M Kawata and M Mikami. Rapid Calculation of Two-Dimensional Ewald Summation. *Chem. Phys. Lett.*, 340:157–164, 2001.

[42] A Arnold, J de Joannis, and C Holm. Electrostatics in Periodic Slab Geometries. I. *J. Chem. Phys.*, 117:2496–2502, 2002.

[43] A Arnold, J de Joannis, and C Holm. Electrostatics in Periodic Slab Geometries. II . *J. Chem. Phys.*, 117:2503–2512, 2002.

[44] S Yi, C Pan, and Z Hu. Note: A Pairwise Form of The Ewald Sum for Non-Neutral Systems. *J. Chem. Phys.*, 147:126101, 2017.

[45] A P dos Santos, M Girotto, and Y Levin. Simulations of Polyelectrolyte Adsorption to a Dielectric Like-Charged Surface. *J. Phys. Chem. B*, 120:10387–10393, 2016.

[46] T Nagy, D Henderson, and D Boda. Simulation of an Electrical Double Layer Model with a Low Dielectric Layer between the Electrode and the Electrolyte. *J. Phys. Chem. B*, 115:11409–11419, 2011.

[47] Zhi-Yong Wang and Zengwei Ma. Examining the Contributions of Image-Charge Forces to Charge Reversal: Discrete Versus Continuum Modeling of Surface Charges. *J. Chem. Theory Comput.*, 12:2880–2888, 2016.

[48] M Girotto, A P dos Santos, and Yan Levin. Interaction of Charged Colloidal Particles at the Water-Air Interface. *J. Phys. Chem. B*, 120:5817–5822, 2016.

[49] G Guerrero-García, Y Jing, and M de la Cruz. Enhancing and Reversing the Electric Field at The Oil–Water Interface with Size-Asymmetric Monovalent Ions. *Soft Matter*, 9:6046–6052, 2013.

[50] A Bakhshandeh, A P dos Santos, and Y Levin. Weak and Strong Coupling Theories for Polarizable Colloids and Nanoparticles. *Phys. Rev. Lett.*, 107:107801, 2011.

[51] A P dos Santos, A Bakhshandeh, and Y Levin. Effects of The Dielectric Discontinuity on The Counterion Distribution in a Colloidal Suspension. *J. Chem. Phys.*, 135:044124, 2011.

[52] A Diehl, A P dos Santos, and Y Levin. Surface Tension of Electrolyte-Air Interface: A Monte Carlo Study. *J. Phys.: Condens. Matt.*, 24:284115, 2012.

[53] J I Siepmann and M Sprik. Influence of Surface Topology and Electrostatic Potential on Water/Electrode Systems. *J. Chem. Phys.*, 102:511–524, 1995.

[54] J Zwanikken and M de la Cruz. Tunable Soft Structure in Charged Fluids Confined by Dielectric Interfaces. *Proc. Natl. Acad. Sci. U.S.A.*, 110:5301–5308, 2013.

[55] V Jadhao, F Solis, and M de la Cruz. Simulation of Charged Systems in Heterogeneous Dielectric Media via a True Energy Functional. *Phys. Rev. Lett.*, 109:223905, 2012.

[56] C Merlet, D T Limmer, M Salanne, R van Roij, P A Madden, D Chandler, and B Rotenberg. The Electric Double Layer Has a Life of Its Own. *J. Phys. Chem. C*, 118:18291–18298, 2014.

[57] D T Limmer, C Merlet, M Sallane, D Chandler, P A Madden, R van Roij, and B Rotenberg. Charge Fluctuations in Nanoscale Capacitors. *Phys. Rev. Lett.*, 111:106102–106106, 2013.

[58] Y Jing, V Jadhao, J Zwanikken, and M de La Cruz. Ionic Structure in Liquids Confined by Dielectric Surfaces. *J. Chem. Phys.*, 143:194508, 2015.

[59] Z Gan, H Wu, K Barros, Z Xu, and E Luijten. Comparison of Efficient Techniques for The Simulation of Dielectric Objects in Electrolytes. *J. Comp. Phys.*, 291:317–333, 2015.

[60] S Tyagi, M Süzen, M Sega, M Barbosa, S Kantarovitch, and C Holm. An Iterative, Fast, Linear-Scaling Method for Computing Induced Charges on Arbitrary Dielectric Boundaries. *J. Chem. Phys.*, 132:154112, 2010.

[61] A Arnold, K Breitsprecher, F Fahrenberger, S Kesselheim, O Lenz, and C Holm. Efficient Algorithms for Electrostatic Interactions Including Dielectric Contrasts. *Entropy*, 15:4569–4588, 2013.

[62] S Tyagi, A Arnold, and C Holm. ICMMM2D: An Accurate Method to Include Planar Dielectric Interfaces via Image Charge Summation. *J. Chem. Phys.*, 127:154723, 2007.

[63] S Tyagi, A Arnold, and C Holm. Electrostatic Layer Correction with Image Charges: A Linear Scaling Method to Treat Slab 2D+h Systems with Dielectric Interfaces. *J. Chem. Phys.*, 129:204102, 2008.

[64] D Boda, D Gillespie, W Nonner, D Henderson, and B Eisenberg. Computing Induced Charges in Inhomogeneous Dielectric Media: Application in a Monte Carlo Simulation of Complex Ionic Systems. *Phys. Rev. E*, 69:046702, 2004.

[65] M Armand, F Endres, D R MacFarlane, H Ohno, and B Scrosati. Ionic-Liquid Materials for The Electrochemical Challenges of the Future. *Nat. Mat.*, 8:621–629, 2009.

[66] X Kong, D Lu, Z Liu, and J Wu. Molecular Dynamics for the Charging Behavior of Nanostructured Electric Double Layer Capacitors containing Room Temperature Ionic Liquids. *Nano Research*, 8:931–940, 2015.

[67] S. Kondrat and A. Kornyshev. Superionic State in Double-Layer Capacitors with Nanoporous Electrodes. *J. Phys.: Condens. Matter*, 23(2):022201, 2011.

[68] P Simon and Y Gogotsi. Materials For Electrochemical Capacitors. *Nat. Mat.*, 7:845–854, 2008.

[69] M Chen, S Li, and G Feng. The Influence of Anion Shape on the Electrical Double Layer Microstructure and Capacitance of Ionic Liquids-Based Supercapacitors by Molecular Simulations. *Molecules*, 22:241–242, 2017.

[70] S Ito, S M Zakeeruddin, P Comte, P Liska, D Kuang, and M Grätzel. Bifacial Dye-Sensitized Solar Cells Based on an Ionic Liquid Electrolyte. *Nat. Photonics*, 2:693–698, 2008.

[71] Q Li, Q Tang, B He, and P Yang. Full Ionic-Liquid Gel Electrolytes: Enhanced Photovoltaic Performances in Dye-Sensitized Solar Cells. *J. Power Sources*, 264:83–91, 2014.

[72] J Wishart. Energy Applications of Ionic Liquids. *Energy Environ. Sci.*, 2:956–961, 2009.

[73] F Zhou, Y Liang, and W Liu. Ionic Liquid Lubricants: Designed Chemistry for Engineering Applications. *Chem. Soc. Rev.*, 38:2590–2599, 2009.

[74] M Girotto, A P dos Santos, and Y Levin. Simulations of Ionic Liquids Confined by Metal Electrodes Using Periodic Green Functions. *J. Chem. Phys.*, 147:074109, 2017.

[75] A P dos Santos, M Girotto, and Y Levin. Simulations of Coulomb Systems Confined by Polarizable Surfaces Using Periodic Green Functions. *J. Chem. Phys.*, 147:184105, 2017.

[76] T Laino and J Hutter. Notes on "Ewald summation of electrostatic multipole interactions up to quadrupolar level" [J. Chem. Phys. 119, 7471 (2003)] . *J. Chem. Phys.*, 129:074102, 2008.

[77] J Stenhammar, M Trulsson, and P Linse. Some Comments and Corrections Regarding The Calculation of Electrostatic Potential Derivatives Using The Ewald Summation Technique. *J. Chem. Phys.*, 134:224104, 2011.

[78] E R Smith. Electrostatic Energy in Ionic Crystals. *Proc. R. Soc. London A*, 375:475–505, 1981.

[79] Russel, W. B., Saville, D. A. and Schowalter, W. R. *Colloidal Dispersions*. Cambridge University Press, New York, United States of America, 1989.

[80] J D Jackson. *Classical Electrodynamics*. Wyley, California, United States of America, 1999.

[81] K Kiyohara and K Asaka. Monte Carlo Simulation of Electrolytes in The Constant Voltage Ensemble. *J. Chem. Phys.*, 126:214704–214717, 2007.

[82] Y Levin. Electrostatics of Ions Inside The Nanopores and Trans-Membrane Channels. *Europhys. Lett.*, 76:163, 2006.

[83] V Kobelev, A B Kolomeisky, and M E Fisher. Lattice Models of Ionic Systems. *J. Chem. Phys.*, 116:7589–7598, 2002.

[84] M C Lonergan, J W Perram, M A Ratner, and D F Shriver. Monte Carlo Investigations of Coloumbic Correlations in Lattice Gas Models. *J. Chem. Phys.*, 98:4937–4947, 1993.

[85] H Bartsch, O Dannenmann, and M Bier. Thermal and Structural Properties of Ionic Fluids. *Phys. Rev. E*, 91:042146–042153, 2015.

[86] A Panagiotopoulos. Large Lattice Discretization Effects on the Phase Coexistence of Ionic Liquids. *Phys. Rev. Lett.*, 83:2981–2984, 1999.

[87] P Wasserscheid and T Welton and Eds. *Ionic Liquids in Synthesis*. Wiley-VCH, Weinheim, Germany, 2003.

[88] M N Kobrak. The Relationship between Solvent Polarity and Molar Volume in Room-Temperature Ionic Liquids. *Green Chem.*, 10:80–86, 2008.

[89] M.-M Huang, Y Jiang, P Sasisanker, G W Driver, and H Weingartner. Static Relative Dielectric Permittivities of Ionic Liquids at 25° C. *J. Chem. Eng. Data*, 56:1494–1499, 2011.

[90] J MacDonald and C Barlow Jr. Theory of Double Layer Differential Capacitance in Electrolytes. *J. Chem. Phys.*, 36:3062–3080, 1962.

[91] K Breitsprecher, P Košovan, and C Holm. Coarse-Grained Simulations of an Ionic Liquid-Based Capacitor: I. Density, Ion Size, and Valency Effects. *J. Phys.: Cond. Matt.*, 26:284108–284121, 2014.

[92] K Breitsprecher, P Košovan, and C Holm. Coarse-Grained Simulations of an Ionic Liquid-Based Capacitor: II. Assymetry in Ion Shape and Charge Localization. *J. Phys.: Cond. Matt.*, 26:284114–284121, 2014.

[93] E Marinari and G Parisi. Simulated Tempering: A New Monte Carlo Scheme. *Europhys. Lett.*, 19:451–458, 1992.

[94] J Liu and E Juijten. Rejection-Free Geometric Cluster Algorithm for Complex Fluid. *Phys. Rev. Let.*, 92:035504, 2004.